

GAN-Supervised Dense Visual Alignment

William Peebles¹ Jun-Yan Zhu² Richard Zhang³ Antonio Torralba⁴ Alexei A. Efros¹ Eli Shechtman³
¹UC Berkeley ²Carnegie Mellon University ³Adobe Research ⁴MIT CSAIL

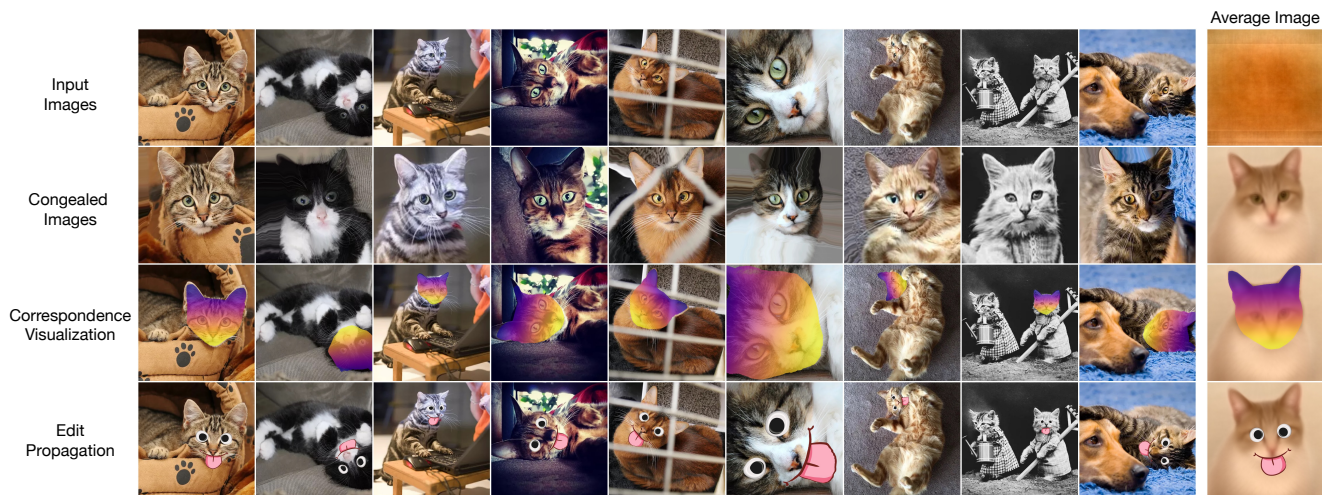


Figure 1. Given an input dataset of unaligned images, our GANgealing algorithm discovers dense correspondences between all images. **Top row:** Images from LSUN Cats and the dataset’s average image. **Second row:** Our learned transformations of the input images. **Third row:** Dense correspondences learned by GANgealing. **Bottom row:** By annotating the average transformed image, we can propagate user edits to images and videos. Please see our project page for detailed video results: www.wpeebles.com/gangealing.

Abstract

We propose *GAN-Supervised Learning*, a framework for learning discriminative models and their GAN-generated training data jointly end-to-end. We apply our framework to the dense visual alignment problem. Inspired by the classic Congealing method, our GANgealing algorithm trains a Spatial Transformer to map random samples from a GAN trained on unaligned data to a common, jointly-learned target mode. We show results on eight datasets, all of which demonstrate our method successfully aligns complex data and discovers dense correspondences. GANgealing significantly outperforms past self-supervised correspondence algorithms and performs on-par with (and sometimes exceeds) state-of-the-art supervised correspondence algorithms on several datasets—without making use of any correspondence supervision or data augmentation and despite being trained exclusively on GAN-generated data. For precise correspondence, we improve upon state-of-the-art supervised methods by as much as 3×. We show applications of our method for augmented reality, image editing and automated pre-processing of image datasets for downstream GAN training.

1. Introduction

Visual alignment, also known as the correspondence or registration problem, is a critical element in much of computer vision, including optical flow, 3D matching, medical imaging, tracking and augmented reality. While much recent progress has been made on pairwise alignment (aligning image A to image B) [2, 14, 22, 33, 50, 56, 57, 59, 66–69, 72], the problem of global joint alignment (aligning all images across a dataset) has not received as much attention. Yet, joint alignment is crucial for tasks requiring a common reference frame, such as automatic keypoint annotation, augmented reality or edit propagation (see Figure 1 bottom row). There is also evidence that training on jointly aligned datasets (such as FFHQ [41], AFHQ [15], CelebA-HQ [39]) can produce higher quality generative models than training on unaligned data.

In this paper, we take inspiration from a series of classic works on automatic joint image set alignment. In particular, we are motivated by the seminal unsupervised *Congealing* method of Learned-Miller [47] which showed that a set of images could be brought into alignment by continually warping them toward a common, updating mode. While Congeal-

Code and models: www.github.com/wpeebles/gangealing

ing can work surprisingly well on simple binary images, such as MNIST digits, the direct pixel-level alignment is not powerful enough to handle most datasets with significant appearance and pose variation.

To address these limitations, we propose GANgealing: a *GAN-Supervised* algorithm that learns transformations of input images to bring them into better joint alignment. The key is in employing the latent space of a GAN (trained on the unaligned data) to automatically generate paired training data for a Spatial Transformer [34]. Crucially, in our proposed GAN-Supervised Learning framework, *both* the Spatial Transformer and the target images are learned jointly. Our Spatial Transformer is trained *exclusively* with GAN images and generalizes to real images at test time.

We show results spanning eight datasets—LSUN Bicycles, Cats, Cars, Dogs, Horses and TVs [84], In-The-Wild CelebA [51] and CUB [80]—that demonstrate our GANgealing algorithm is able to discover accurate, dense correspondences across datasets. We show our Spatial Transformers are useful in image editing and augmented reality tasks. Quantitatively, GANgealing significantly outperforms past self-supervised dense correspondence methods, nearly doubling key point transfer accuracy (PCK [4]) on many SPair-71K [58] categories. Moreover, GANgealing sometimes matches and even exceeds state-of-the-art correspondence-*supervised* methods.

2. Related Work

Pre-Trained GANs for Vision. Prior work has explored the use of GANs [27, 65] in vision tasks such as classification [10, 12, 54, 71, 81], segmentation [55, 76, 79, 87] and representation learning [7, 20, 21, 23, 35]. Likewise, we share the goal of leveraging the power of pre-trained deep generative models for vision tasks. However, the relevant past methods follow a common two-stage paradigm of (1) synthesizing a GAN-generated dataset and (2) training a discriminative model on the fixed dataset. In contrast, our GAN-Supervised Learning approach learns *both* the discriminative model as well as the GAN-generated data jointly end-to-end. We do not rely on hand-crafted pixel space augmentations [12, 35], human-labeled data [76, 86, 87] or post-processing of GAN-generated datasets using domain knowledge [10, 55, 79, 86].

Joint Image Set Alignment. Average images have long been used to visualize joint alignment of image sets of the same semantic content (e.g., [75, 92]), with the seminal work of Congealing [31, 47] establishing unsupervised joint alignment as a research problem. Congealing uses sequential optimization to gradually minimize the entropy of the intensity distribution of a set of images by continuously warping each image via a parametric transformation (e.g., affine). It produces impressive results on well-structured datasets, such as digits, but struggles with more complex data. Subse-

quent work in this area assumes the data lies on a low-rank subspace [43, 64] or factorizes images as a composition of color, appearance and shape [61] to establish dense correspondences between instances of the same object category. FlowWeb [89] uses cycle consistency constraints to estimate a fully-connected correspondence flow graph. Every method above assumes that it is possible to align all images to a single central mode in the data. Joint visual alignment and clustering was proposed in AverageExplorer [92] but as a user-driven data interaction tool. Bounding box supervision has been used to align and cluster multiple modes within object categories [19]. Automated transformation-invariant clustering methods [24, 25] can align images in a collection before comparing them but work only in limited domains. Recently, Monnier et al. [62] showed that warps could be predicted with a network instead, removing the need for per-image optimization; this opened the door for simultaneous alignment and clustering of large-scale collections. Unlike our approach, these methods assume images can be aligned with simple (e.g., affine) color transformations; this assumption breaks down for complex datasets like LSUN.

Spatial Transformer Networks (STNs). A Spatial Transformer module [34] is one way to incorporate learnable geometric transformations in a deep learning framework. It regresses a set of warp parameters, where the warp and grid sampling functions are differentiable to enable backpropagation. STNs have seen success in discriminative tasks (e.g., classification) and applications such as robust filter learning [16, 36], view synthesis [26, 63, 90] and 3D representation learning [38, 83, 88]. Inverse Compositional STNs (IC-STNs) [48] advocate an iterative image alignment framework in the spirit of the classical Lukas-Kanade algorithm [6, 53]. Prior work has incorporated STNs in generative models for geometry-texture disentanglement [82] and image compositing [49]. In contrast, we use a generative model to directly produce training data *for* STNs.

3. GAN-Supervised Learning

In this section, we present GAN-Supervised Learning. Under this framework, (\mathbf{x}, \mathbf{y}) pairs are sampled from a pre-trained GAN generator, where \mathbf{x} is a random sample from the GAN and \mathbf{y} is the sample obtained by applying a *learned* latent manipulation to \mathbf{x} 's latent code. These pairs are used to train a network $f_\theta : \mathbf{x} \rightarrow \mathbf{y}$. This framework minimizes the following loss:

$$\mathcal{L}(f_\theta, \mathbf{y}) = \ell(f_\theta(\mathbf{x}), \mathbf{y}), \quad (1)$$

where ℓ is a reconstruction loss. In vanilla supervised learning, f_θ is learned on *fixed* (\mathbf{x}, \mathbf{y}) pairs. In contrast, in GAN-Supervised Learning, *both* f_θ and the targets \mathbf{y} are learned jointly end-to-end. At test time, we are free to evaluate f_θ on *real* inputs.

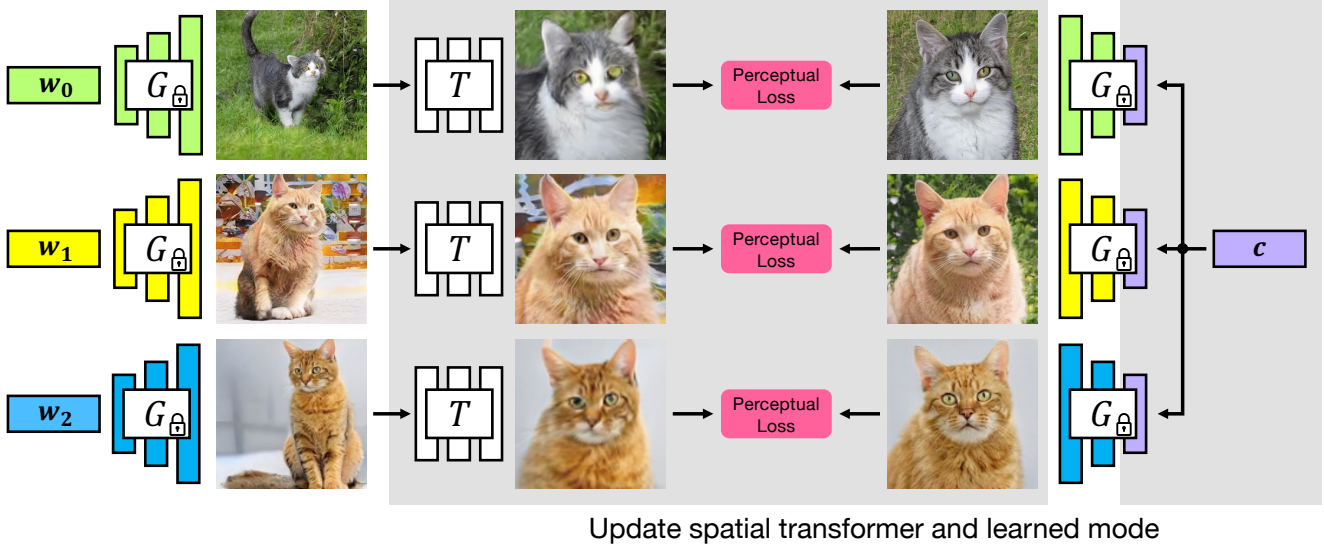


Figure 2. **GANgealing Overview.** We first train a generator G on unaligned data. We create a *synthetically-generated* dataset for alignment by learning a mode \mathbf{c} in the generator’s latent space. We use this dataset to train a Spatial Transformer Network T to map from unaligned to corresponding aligned images using a perceptual loss [37]. The Spatial Transformer generalizes to align *real* images automatically.

3.1. Dense Visual Alignment

Here, we show how GAN-Supervised Learning can be applied to Congealing [47]—a classic unsupervised alignment algorithm. In this instantiation, f_θ is a Spatial Transformer Network [34] T , and we describe our parameterization of inputs \mathbf{x} and learned targets \mathbf{y} below. We call our algorithm *GANgealing*. We present an overview in Figure 2.

GANgealing begins by training a latent variable generative model G on an unaligned input dataset. We refer to the input latent vector to G as $\mathbf{w} \in \mathbb{R}^{512}$. With G trained, we are free to draw samples from the unaligned distribution by computing $\mathbf{x} = G(\mathbf{w})$ for randomly sampled $\mathbf{w} \sim \mathcal{W}$, where \mathcal{W} denotes the distribution over latents. Now, consider a fixed latent vector $\mathbf{c} \in \mathbb{R}^{512}$. This vector corresponds to a fixed synthetic image $G(\mathbf{c})$ from the original unaligned distribution. A simple idea in the vein of traditional Congealing is to use $G(\mathbf{c})$ as the target mode \mathbf{y} —i.e., we learn a Spatial Transformer T that is trained to warp every random unaligned image $\mathbf{x} = G(\mathbf{w})$ to the same target image $\mathbf{y} = G(\mathbf{c})$. Since G is differentiable in its input, we can optimize \mathbf{c} and hence learn the target we wish to congeal towards. Specifically, we can optimize the following loss with respect to both T ’s parameters and the target image’s latent vector \mathbf{c} jointly:

$$\mathcal{L}_{\text{align}}(T, \mathbf{c}) = \ell(T(G(\mathbf{w})), G(\mathbf{c})), \quad (2)$$

where ℓ is some distance function between two images. By minimizing \mathcal{L} with respect to the target latent vector \mathbf{c} , GANgealing encourages \mathbf{c} to find a pose that makes T ’s

job as easy as possible. If the current value of \mathbf{c} corresponds to a pose that cannot be reached from most images via the transformations predicted by T , then it can be adjusted via gradient descent to a different vector that is “reachable” by more images.

This simple approach is reasonable for datasets with limited diversity; however, in the presence of significant appearance and pose variation, it is not reasonable to expect that every unaligned sample can be aligned to the exact same target image. Hence, optimizing the above loss does not produce good results in general (see Table 3). Instead of using the same target $G(\mathbf{c})$ for every randomly sampled image $G(\mathbf{w})$, it would be ideal if we could construct a *per-sample target* that retains the appearance of $G(\mathbf{w})$ but where the pose and orientation of the object in the target image is roughly identical across targets. To accomplish this, given $G(\mathbf{w})$, we produce the corresponding target by setting just a portion of the \mathbf{w} vector equal to the target vector \mathbf{c} . Specifically, let $\text{mix}(\mathbf{c}, \mathbf{w}) \in \mathbb{R}^{512}$ refer to the latent vector whose first entries are taken from \mathbf{c} and remaining entries are taken from \mathbf{w} . By sampling new \mathbf{w} vectors, we can create an infinite pool of paired data where the input is the unaligned image $\mathbf{x} = G(\mathbf{w})$ and the target $\mathbf{y} = G(\text{mix}(\mathbf{c}, \mathbf{w}))$ shares the appearance of $G(\mathbf{w})$ but is in a learned, fixed pose. This gives rise to the GANgealing loss function:

$$\mathcal{L}_{\text{align}}(T, \mathbf{c}) = \ell(\underbrace{T(G(\mathbf{w}))}_{\mathbf{x}}, \underbrace{G(\text{mix}(\mathbf{c}, \mathbf{w}))}_{\mathbf{y}}), \quad (3)$$

where ℓ is a perceptual loss function [37]. In this paper, we

opt to use StyleGAN2 [42] as our choice of G , but in principle other GAN architectures could be used with our method. An advantage of using StyleGAN2 is that it possesses some innate style-pose disentanglement that we can leverage to construct the per-image target described above. Specifically, we can construct the per-sample targets $G(\text{mix}(\mathbf{c}, \mathbf{w}))$ by using style mixing [41]— \mathbf{c} is supplied to the first few inputs to the synthesis generator that roughly control pose and \mathbf{w} is fed into the later layers that roughly control texture. See Table 3 for a quantitative ablation of the mixing "cutoff point" where we begin to feed in \mathbf{w} (i.e., the cutoff point is chosen as a layer index in \mathcal{W}^+ space [1]).

Spatial Transformer Parameterization. Recall that a Spatial Transformer T takes as input an image and regresses and applies a (reverse) sampling grid $\mathbf{g} \in \mathbb{R}^{H \times W \times 2}$ to the input image. Hence, one must choose how to constrain the \mathbf{g} regressed by T . In this paper, we explore a T that performs similarity transformations (rotation, uniform scale, horizontal shift and vertical shift). We also explore an arbitrarily expressive T that directly regresses unconstrained per-pixel flow fields \mathbf{g} . Our final T is a composition of the similarity Spatial Transformer into the unconstrained Spatial Transformer, which we found worked best. In contrast to prior work [49, 62], we do not find multi-stage training necessary and train our composed T end-to-end. Finally, our Spatial Transformer is also capable of performing horizontal flips at test time—please refer to Appendix B.4 for details.

When using the unconstrained T , it can be beneficial to add a total variation regularizer that encourages the predicted flow to be smooth to mitigate degenerate solutions: $\mathcal{L}_{\text{TV}}(T) = \mathcal{L}_{\text{Huber}}(\Delta_x \mathbf{g}) + \mathcal{L}_{\text{Huber}}(\Delta_y \mathbf{g})$, where $\mathcal{L}_{\text{Huber}}$ denotes the Huber loss and Δ_x and Δ_y denote the partial derivative w.r.t. x and y coordinates under finite differences. We also use a regularizer that encourages the flow to not deviate from the identity transformation: $\mathcal{L}_1(T) = \|\mathbf{g}\|_2^2$.

Parameterization of \mathbf{c} . In practice, we do not backpropagate gradients directly into \mathbf{c} . Instead, we parameterize \mathbf{c} as a linear combination of the top- N principal directions of \mathcal{W} space [28, 74]:

$$\mathbf{c} = \bar{\mathbf{w}} + \sum_{i=1}^N \alpha_i \mathbf{d}_i, \quad (4)$$

where $\bar{\mathbf{w}}$ is the empirical mean \mathbf{w} vector, \mathbf{d}_i is the i -th principal direction and α_i is the learned scalar coefficient of the direction. Instead of optimizing \mathcal{L} w.r.t. \mathbf{c} directly, we optimize it w.r.t. the coefficients $\{\alpha_i\}_{i=1}^N$. The motivation for this reparameterization is that StyleGAN’s \mathcal{W} space is highly expressive, and hence it can easily navigate off the manifold of natural images in the absence of additional constraints, violating our desired constraint that the target images are re-

alistic. Decreasing N keeps \mathbf{c} on the manifold and prevents degenerate solutions. See Table 3 for an ablation of N .

Our final GANgealing objective is given by:

$$\mathcal{L}(T, \mathbf{c}) = \mathbb{E}_{\mathbf{w} \sim \mathcal{W}} [\mathcal{L}_{\text{align}}(T, \mathbf{c}) + \lambda_{\text{TV}} \mathcal{L}_{\text{TV}}(T) + \lambda_I \mathcal{L}_I(T)]. \quad (5)$$

We set the loss weighting λ_{TV} at either 1000 or 2500 (depending on choice of ℓ) and the loss weighting λ_I at 1. See Appendix B for additional details and hyperparameters.

3.2. Joint Alignment and Clustering

GANgealing as described so far can handle highly-multimodal data (e.g., LSUN Bicycles, Cats, etc.). Some datasets, such as LSUN Horses, feature extremely diverse poses that cannot be represented well by a single mode in the data. To handle this situation, GANgealing can be adapted into a clustering algorithm by simply learning more than one target latent \mathbf{c} . Let K refer to the number of \mathbf{c} vectors (clusters) we wish to learn. Since each \mathbf{c} captures a specific mode in the data, learning multiple $\{\mathbf{c}_k\}_{k=1}^K$ would enable us to learn multiple modes. Now, each \mathbf{c}_k will learn its own set of α coefficients. Similarly, we will now have K Spatial Transformers, one for each mode being learned. This variant of GANgealing amounts to simultaneously clustering the data and learning dense correspondence between all images within each cluster. To encourage each \mathbf{c}_k and T_k pair to specialize in a particular mode, we include a hard-assignment step to assign unaligned synthetic images to modes:

$$\mathcal{L}_{\text{align}}^K(T, \mathbf{c}) = \min_k \mathcal{L}_{\text{align}}(T_k, \mathbf{c}_k) \quad (6)$$

Note that the $K = 1$ case is equivalent to the previously described unimodal case. At test time, we can assign an input fake image $G(\mathbf{w})$ to its corresponding cluster index $k^* = \arg \min_k \mathcal{L}_{\text{align}}(T_k, \mathbf{c}_k)$. Then, we can warp it with the Spatial Transformer T_{k^*} . However, a problem arises in that we cannot compute this cluster assignment for input *real* images—the assignment step requires computing $\mathcal{L}_{\text{align}}$, which itself requires knowledge of the input image’s corresponding \mathbf{w} vector. The most obvious solution to this problem is to perform GAN inversion [8, 11, 91] on input real images \mathbf{x} to obtain a latent vector \mathbf{w} such that $G(\mathbf{w}) \approx \mathbf{x}$. However, accurate GAN inversion for non-face datasets remains somewhat challenging and slow, despite recent progress [3, 32]. Instead, we opt to train a classifier that directly predicts the cluster assignment of an input image. We train the classifier using a standard cross-entropy loss on (input fake image, target cluster) pairs $(G(\mathbf{w}), k^*)$, where k^* is obtained using the above assignment step. We initialize the classifier with the weights of T (replacing the warp head with a randomly-initialized classification head). As with the Spatial Transformer, the classifier generalizes well to real images despite being trained exclusively on fake samples.

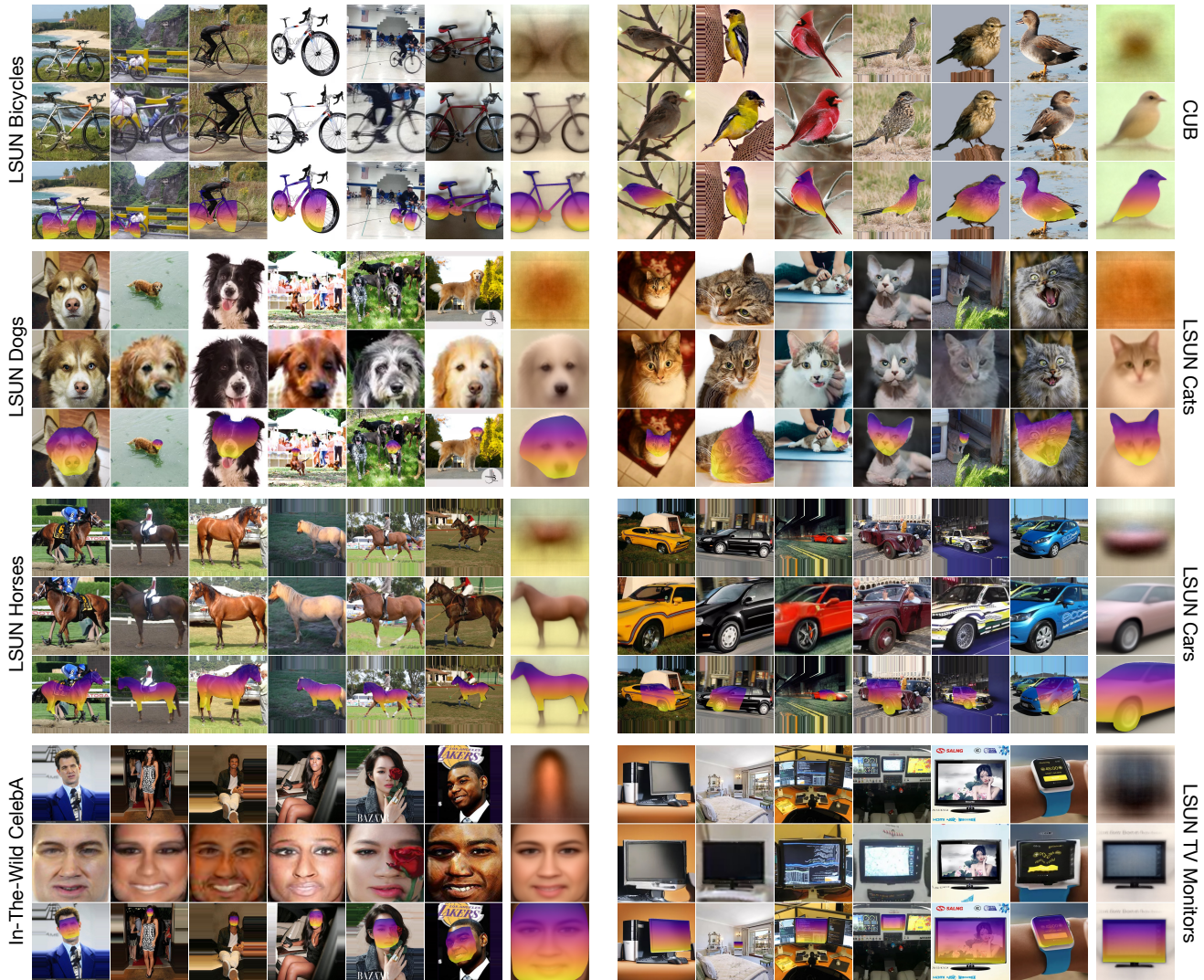


Figure 3. **Dense correspondence results on eight datasets.** For each dataset, the top row shows unaligned images and the dataset average image. The middle row shows our learned transformations of the input images. The bottom row shows dense correspondences between the images. For our clustering models (LSUN Horses and Cars), we show results for one selected cluster.

4. Experiments

In this section, we present quantitative and qualitative results of GANgealing on eight datasets: LSUN Bicycles, Cats, Cars, Dogs, Horses and TVs [84], In-The-Wild CelebA [51] and CUB-200-2011 [80]. These datasets feature significant diversity in appearance, pose and occlusion of objects. Only LSUN Cars and Horses use clustering ($K = 4$)¹; for all other datasets we use unimodal GANgealing ($K = 1$). Note that all figures except Figure 2 show our method applied to real images—not GAN samples. Please see www.wpeebles.com/gangealing for full results.

¹ K is a hyperparameter that can be set by the user. We found $K = 4$ to be a good default choice for our clustering models.

4.1. Propagation from Congealed Space

With the Spatial Transformer T trained, it is trivial to identify dense correspondences between real input images x . A particularly convenient way to find dense correspondences between a set of images is by propagating from our *congealed coordinate space*. As described earlier, T both regresses and applies a sampling grid g to an input image. Because we use reverse sampling, this grid tells us where each point in the congealed image $T(x)$ maps to in the original image x . This enables us to propagate *anything* from the congealed coordinate space—dense labels, sparse keypoints, etc. If a user annotates a *single* congealed image (or the average congealed image) they can then propagate those labels to an entire dataset by simply predicting the grid g for each im-

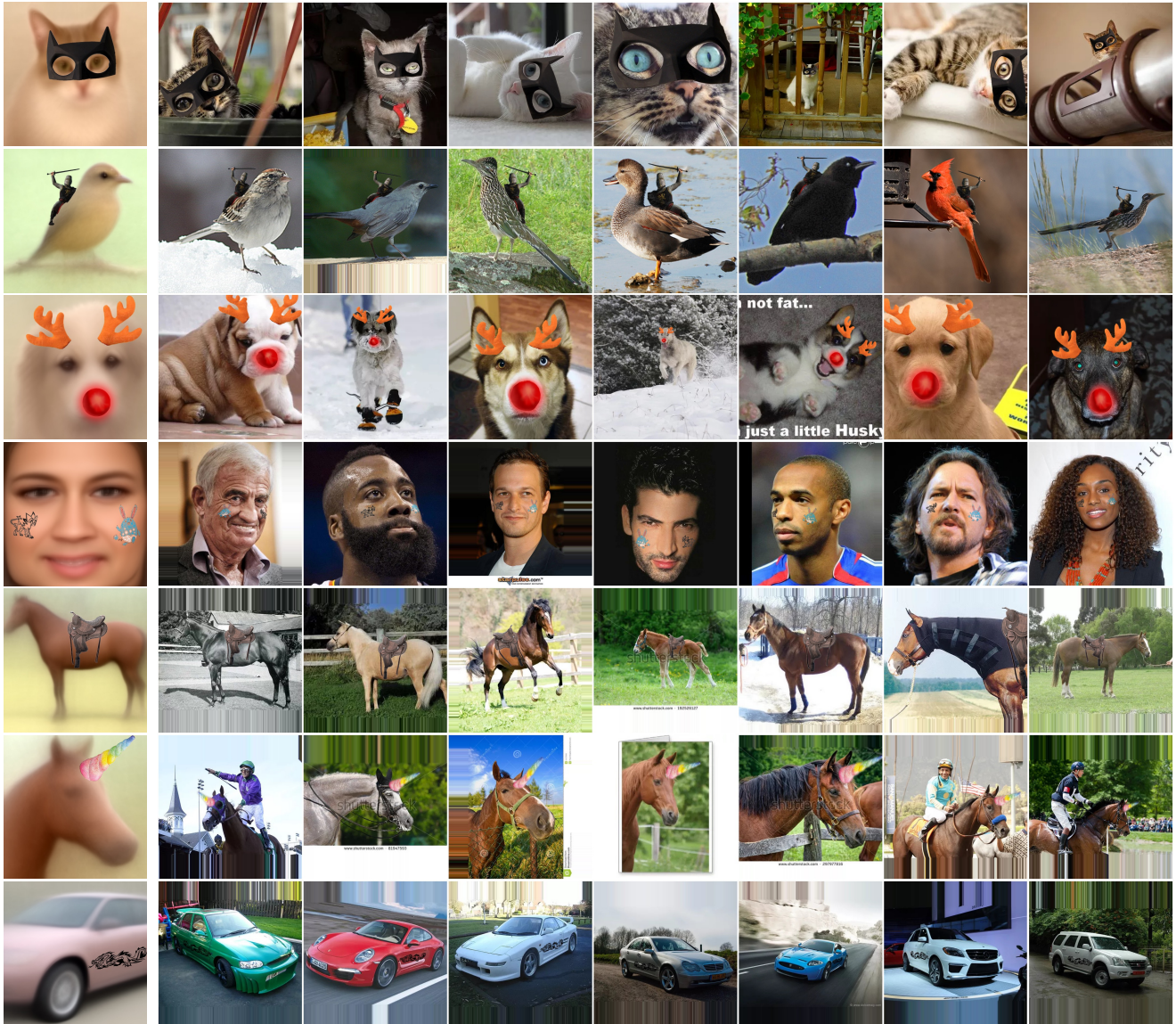


Figure 4. **Image editing with GANgealing.** By annotating just a single image per-category (our average transformed image), a user can propagate their edits to any image or video in the same category.

age x in their dataset via a forward pass through T . Figures 1 and 3 show visual results for all eight datasets—our method can find accurate dense correspondences in the presence of significant appearance and pose diversity. GANgealing accurately handles diverse morphologies of birds, cats with varying facial expressions and bikes in different orientations.

Image Editing. Our average congealed image is a template that can propagate any user edit to images of the same category. For example, by drawing cartoon eyes or overlaying a Batman mask on our average congealed cat, a user can effortlessly propagate their edits to massive numbers of cat images with forward passes of T . We show editing results on several datasets in Figures 4 and 1.

Augmented Reality. Just as we can propagate dense correspondences to images, we can also propagate to individual video frames. Surprisingly, we find that GANgealing yields remarkably smooth and consistent results when applied *out-of-the-box* to videos per-frame without leveraging any temporal information. This enables mixed reality applications such as dense tracking and filters. Please see www.wpeebles.com/gangealing for results.

4.2. Direct Image-to-Image Correspondence

In addition to propagating correspondences from congealed space to unaligned images, we can also find dense correspondences directly between any pair of images x_A and x_B . At a high-level, this merely involves applying the

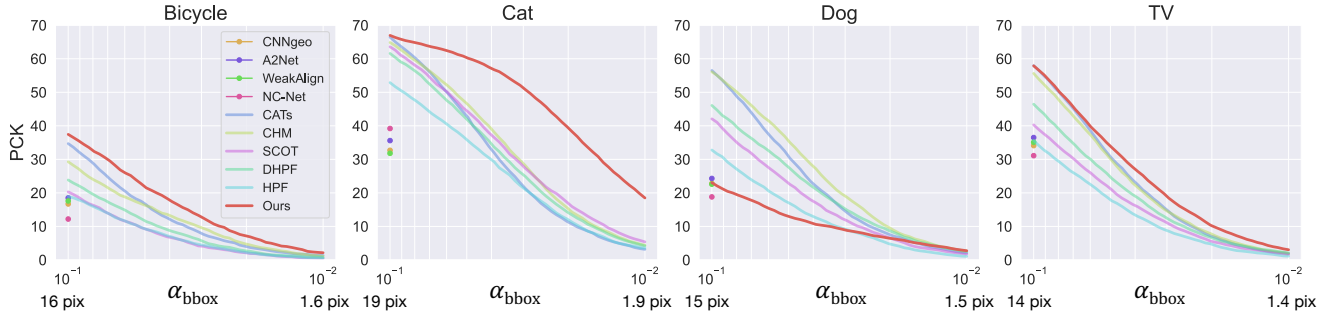


Figure 5. **PCK@ α_{bbox} on various SPair-71K categories for α_{bbox} between 10^{-1} and 10^{-2} .** We report the average threshold (maximum distance for a correspondence to be deemed correct) in pixels for 256×256 images beneath each plot. GANgealing outperforms state-of-the-art supervised methods for very precise thresholds (< 2 pixel error tolerance), sometimes by substantial margins.

forward warp that maps points in x_A to points in $T(x_A)$ and composing it with the reverse warp that maps points in the congealed coordinate space back to x_B . Please refer to Appendix B.7 for details.

Quantitative Results. We evaluate GANgealing with PCK-Transfer. Given a source image x_A , target image x_B and ground-truth keypoints for both images, PCK-Transfer measures the percentage of keypoints transferred from x_A to x_B that lie within a certain radius of the ground-truth keypoints in x_B .

We evaluate PCK on SPair-71K [58] and CUB. For SPair, we use the α_{bbox} threshold in keeping with prior works. Under this threshold, a predicted keypoint is deemed to be correctly transferred if it is within a radius $\alpha_{\text{bbox}} \max(H_{\text{bbox}}, W_{\text{bbox}})$ of the ground truth, where H_{bbox} and W_{bbox} are the height and width of the object bounding box in the target image. For each SPair category, we train a StyleGAN2 on the corresponding LSUN category²—the GANs are trained on 256×256 center-cropped images. We then train a Spatial Transformer using GANgealing and directly evaluate on SPair. For CUB, we first pre-train a StyleGAN2 with ADA [40] on the NABirds dataset [78] and fine-tune it with Freezed [60] on the training split of CUB, using the same image pre-processing and dataset splits as ACSM [45] for a fair comparison. When T performs a horizontal flip for one image in a pair, we permute our model’s predictions for keypoints with a left versus right distinction.

SPair-71K Results. We compare against several self-supervised and state-of-the-art supervised methods on the challenging SPair-71K dataset in Table 1, using the standard $\alpha_{\text{bbox}} = 0.1$ threshold. Our method significantly outperforms prior self-supervised methods on several categories,

²We use off-the-shelf StyleGAN2 models for LSUN Cats, Dogs and Horses. Note that we do not evaluate PCK on our clustering models (LSUN Cars and Horses) as these models can only transfer points between images in the same cluster.

Method	Correspondence Supervision	SPair-71K Category			
		Bicycle	Cat	Dog	TV
HPF [57]	matching pairs + keypoints	18.9	52.9	32.8	35.6
DHPF [59]	matching pairs + keypoints	23.8	61.6	46.1	46.5
SCOT [50]	matching pairs + keypoints*	20.7	63.1	42.5	40.8
CHM [56]	matching pairs + keypoints	29.3	64.9	56.1	55.6
CATs [14]	matching pairs + keypoints	34.7	66.5	56.5	58.0
WeakAlign [67]	matching image pairs	17.6	31.8	22.6	35.1
NC-Net [68]	matching image pairs	12.2	39.2	18.8	31.1
CNNgeo [66]	self-supervised	16.7	32.7	22.8	34.1
A2Net [69]	self-supervised	18.5	35.6	24.3	36.5
GANgealing	GAN-supervised	37.5	67.0	23.1	57.9

Table 1. **PCK-Transfer@ $\alpha_{\text{bbox}} = 0.1$ results on SPair-71K categories (test split).**

nearly doubling the best prior self-supervised method’s PCK on SPair Bicycles and Cats. GANgealing performs on-par with and even outperforms state-of-the-art correspondence-supervised methods on several categories. We increase the previous best PCK on Bicycles achieved by Cost Aggregation Transformers [14] from 34.7% to 37.5% and perform comparably on Cats and TVs.

High-Precision SPair-71K Results. The usual $\alpha_{\text{bbox}} = 0.1$ threshold used in most papers that report on SPair deems a correspondence correct if it is localized within roughly 10 to 20 pixels of the ground truth for 256×256 images (depending on the SPair category). In Figure 5 we evaluate our model’s performance over a range of thresholds between 0.1 and 0.01 (the latter of which affords a roughly 1 to 2 pixel error tolerance, again depending on SPair category). Our method outperforms all supervised methods at these high-precision thresholds across all four categories tested. In particular, our LSUN Cats model significantly improves the previous best SPair Cats PCK@ $\alpha_{\text{bbox}} = 0.01$ achieved by SCOT [50] from 5.4% to 18.5%. On SPair TVs, we improve the best supervised PCK achieved by Dynamic Hyperpixel Flow [59] from 2.1% to 3.0%. Even on SPair Dogs, where GANgealing is outperformed by every supervised method at low-precision thresholds, we marginally outperform all baselines at the 0.01 threshold.



Figure 6. **GANgealing alignment improves downstream GAN training.** We show random, untruncated samples from StyleGAN2 trained on LSUN Cats versus our aligned LSUN Cats (both models trained from scratch). Our method improves visual fidelity.



Figure 7. **Various failure modes:** significant out-of-plane rotation and complex poses poorly modeled by GANs.

CUB Results. Table 2 shows PCK results on CUB, comparing against several 2D and 3D correspondence methods that use varying amounts of supervision. GANgealing achieves 57.5% PCK, outperforming all past methods that require instance mask supervision and performing comparably with the best correspondence-supervised baseline (58.5%).

Ablations. We ablate several components of GANgealing in Table 3. We find that learning the target mode c is critical for complex datasets; fixing $c = \bar{w}$ dramatically degrades PCK from 67% to 10.6% for our LSUN Cats model. This highlights the value of our GAN-Supervised Learning framework where *both the discriminative model and targets are learned jointly*. We additionally find that our baseline inspired by traditional Congealing (using a single learned target $G(c)$ for all inputs) is highly unstable and degrades PCK to as little as 7.7%. This result demonstrates the importance of our *per-input* alignment targets. We also ablate two choices of the perceptual loss ℓ : an off-the-shelf supervised option (LPIPS [85]) and a fully-unsupervised VGG-16 [70] pre-trained with SimCLR [13] on ImageNet-1K [17] (SSL)—there is no significant difference in performance between the two ($\pm 0.2\%$). Please see Table 3 for more ablations.

4.3. Automated GAN Dataset Pre-Processing

An exciting application of GANgealing is automated dataset pre-processing. Dataset alignment is an important yet costly step for many machine learning methods. GAN training in particular benefits from carefully-aligned and filtered datasets, such as FFHQ [41], AFHQ [15] and CelebA-HQ [39]. We can align input datasets using our similarity

Method	Supervision Required		PCK@0.1
	Inst. Mask	Keypoints	
Rigid-CSM (with keypoints) [46]	✓	✓	45.8
ACSM (with keypoints) [45]	✓	✓	51.0
IMR (with keypoints) [77]	✓	✓	58.5
Dense Equivariance [73]	✓		33.5
Rigid-CSM [46]	✓		36.4
ACSM [45]	✓		42.6
IMR [77]	✓		53.4
Neural Best Buddies [2]			35.1
Neural Best Buddies (with flip heuristic)			37.8
GANgealing			57.5

Table 2. **PCK-Transfer@0.1 on CUB.** Numbers for the 3D methods are reported from [45]. We sample 10,000 random pairs from the CUB validation split as in [45].

Ablation Description	Loss (ℓ)	\mathcal{W}^+ cutoff	λ_{TV}	N	PCK
Don't learn c (fix $c = \bar{w}$)	SSL	5	1000	0	10.6
Unconstrained c optimization	SSL	5	1000	512	0.34
Early style mixing cutoff	SSL	4	1000	1	60.5
Late style mixing cutoff	SSL	6	1000	1	65.0
No style mixing	SSL	14	1000	1	25.9
No style mixing (LPIPS)	LPIPS	14	1000	1	7.74
No \mathcal{L}_{TV} regularizer	SSL	5	0	1	59.0
Lower λ_{TV} (LPIPS)	LPIPS	5	1000	1	66.7
Complete model (SSL)	SSL	5	1000	1	67.2
Complete model (LPIPS)	LPIPS	5	2500	1	67.0

Table 3. **GANgealing ablations for LSUN Cats.** We evaluate on SPair-71K Cats using $\alpha_{\text{bbox}} = 0.1$. SSL refers to using a self-supervised VGG-16 as the perceptual loss ℓ . N refers to the number of \mathcal{W} space PCA coefficients learned when optimizing c . Note that the LSUN Cats StyleGAN2 generator has 14 layers.

Spatial Transformer T to train generators with higher visual fidelity. We show results in Figure 6: training StyleGAN2 from scratch with our learned pre-processing of LSUN Cats yields high quality samples reminiscent of AFHQ. As we show in Appendix E, our pre-processing accelerates GAN training significantly.

5. Limitations and Discussion

Our Spatial Transformer has a few notable failure modes as demonstrated in Figure 7. One limitation with GANgealing is that we can only reliably propagate correspondences that are visible in our learned target mode. For example, the learned mode of our LSUN Dogs model is the upper-body of a dog—this particular model is thus incapable of finding correspondences between, e.g., paws. A potential solution to this problem is to initialize the learned mode with a user-chosen image via GAN inversion that covers all points of interest. Despite this limitation, we obtain competitive results on SPair for some categories where many keypoints are not visible in the learned mode (e.g., cats).

In this paper, we showed that GANs can be used to train highly competitive dense correspondence algorithms from scratch with our proposed GAN-Supervised Learning framework. We hope this paper will lead to increased adoption of GAN-Supervision for other challenging tasks.

Acknowledgements. We thank Tim Brooks for his antialiased sampling code and helpful discussions. We thank Tete Xiao, Ilija Radosavovic, Taesung Park, Assaf Shocher, Phillip Isola, Angjoo Kanazawa, Shubham Goel, Allan Jabri, Shubham Tulsiani and Dave Epstein for helpful discussions. This material is based upon work supported by the National Science Foundation Graduate Research Fellowship Program under Grant No. DGE 2146752. Any opinions, findings, and conclusions or recommendations expressed in this material are those of the authors and do not necessarily reflect the views of the National Science Foundation. Additional funding provided by Adobe and Berkeley Deep Drive.

References

- [1] Rameen Abdal, Yipeng Qin, and Peter Wonka. Image2stylegan: How to embed images into the stylegan latent space? In *Proceedings of the IEEE/CVF International Conference on Computer Vision*, pages 4432–4441, 2019. 4
- [2] Kfir Aberman, Jing Liao, Mingyi Shi, Dani Lischinski, Baoquan Chen, and Daniel Cohen-Or. Neural best-buddies: Sparse cross-domain correspondence. *ACM Transactions on Graphics (TOG)*, 37(4):69, 2018. 1, 8
- [3] Yuval Alaluf, Or Patashnik, and Daniel Cohen-Or. Restyle: A residual-based stylegan encoder via iterative refinement. *arXiv preprint arXiv:2104.02699*, 2021. 4
- [4] Mykhaylo Andriluka, Leonid Pishchulin, Peter Gehler, and Bernt Schiele. 2d human pose estimation: New benchmark and state of the art analysis. In *Proceedings of the IEEE Conference on Computer Vision and Pattern Recognition*, pages 3686–3693, 2014. 2
- [5] David Arthur and Sergei Vassilvitskii. k-means++: The advantages of careful seeding. Technical report, Stanford, 2006. 13
- [6] Simon Baker and Iain Matthews. Lucas-kanade 20 years on: A unifying framework. *International journal of computer vision*, 56(3):221–255, 2004. 2
- [7] Manel Baradad, Jonas Wulff, Tongzhou Wang, Phillip Isola, and Antonio Torralba. Learning to see by looking at noise. *arXiv preprint arXiv:2106.05963*, 2021. 2
- [8] David Bau, Hendrik Strobelt, William Peebles, Jonas Wulff, Bolei Zhou, Jun-Yan Zhu, and Antonio Torralba. Semantic photo manipulation with a generative image prior. *ACM Transactions on Graphics (Proceedings of ACM SIGGRAPH)*, 38(4), 2019. 4
- [9] David Bau, Jun-Yan Zhu, Jonas Wulff, William Peebles, Hendrik Strobelt, Bolei Zhou, and Antonio Torralba. Seeing what a gan cannot generate. In *IEEE International Conference on Computer Vision (ICCV)*, 2019. 21
- [10] Victor Besnier, Himalaya Jain, Andrei Bursuc, Matthieu Cord, and Patrick Pérez. This dataset does not exist: training models from generated images. In *ICASSP 2020-2020 IEEE International Conference on Acoustics, Speech and Signal Processing (ICASSP)*, pages 1–5. IEEE, 2020. 2
- [11] Andrew Brock, Theodore Lim, James M Ritchie, and Nick Weston. Neural photo editing with introspective adversarial networks. In *International Conference on Learning Representations (ICLR)*, 2017. 4
- [12] Lucy Chai, Jun-Yan Zhu, Eli Shechtman, Phillip Isola, and Richard Zhang. Ensembling with deep generative views. In *Proceedings of the IEEE/CVF Conference on Computer Vision and Pattern Recognition*, pages 14997–15007, 2021. 2
- [13] Ting Chen, Simon Kornblith, Mohammad Norouzi, and Geoffrey Hinton. A simple framework for contrastive learning of visual representations. In *International conference on machine learning*, pages 1597–1607. PMLR, 2020. 8
- [14] Seokju Cho, Sunghwan Hong, Sangryul Jeon, Yunsung Lee, Kwanghoon Sohn, and Seungryoung Kim. Semantic correspondence with transformers. *arXiv preprint arXiv:2106.02520*, 2021. 1, 7
- [15] Yunjey Choi, Youngjung Uh, Jaejun Yoo, and Jung-Woo Ha. Stargan v2: Diverse image synthesis for multiple domains. In *IEEE Conference on Computer Vision and Pattern Recognition (CVPR)*, 2020. 1, 8, 17
- [16] Jifeng Dai, Haozhi Qi, Yuwen Xiong, Yi Li, Guodong Zhang, Han Hu, and Yichen Wei. Deformable convolutional networks. *arXiv preprint arXiv:1703.06211*, 2017. 2
- [17] Jia Deng, Wei Dong, Richard Socher, Li-Jia Li, Kai Li, and Li Fei-Fei. Imagenet: A large-scale hierarchical image database. In *IEEE Conference on Computer Vision and Pattern Recognition (CVPR)*, 2009. 8
- [18] Terrance DeVries, Michal Drozdal, and Graham W Taylor. Instance selection for gans. *Advances in Neural Information Processing Systems*, 2020. 16
- [19] Santosh Divvala, Alexei Efros, and Martial Hebert. Object instance sharing by enhanced bounding box correspondence. In *BMVC*, 2012. 2
- [20] Jeff Donahue, Philipp Krähenbühl, and Trevor Darrell. Adversarial feature learning. In *International Conference on Learning Representations (ICLR)*, 2017. 2
- [21] Jeff Donahue and Karen Simonyan. Large scale adversarial representation learning. *arXiv preprint arXiv:1907.02544*, 2019. 2
- [22] Alexey Dosovitskiy, Philipp Fischer, Eddy Ilg, Philip Hausser, Caner Hazirbas, Vladimir Golkov, Patrick Van Der Smagt, Daniel Cremers, and Thomas Brox. FlowNet: Learning optical flow with convolutional networks. In *Proceedings of the IEEE international conference on computer vision*, pages 2758–2766, 2015. 1
- [23] Vincent Dumoulin, Ishmael Belghazi, Ben Poole, Alex Lamb, Martin Arjovsky, Olivier Mastropietro, and Aaron Courville. Adversarially learned inference. In *International Conference on Learning Representations (ICLR)*, 2017. 2
- [24] Brendan J. Frey and Nebojsa Jojic. Transformation-invariant clustering using the EM algorithm. *IEEE Transactions on Pattern Analysis and Machine Intelligence (TPAMI)*, 25(1):1–17, 2003. 2
- [25] J. Brendan Frey and Nebojsa Jojic. Estimating mixture models of images and inferring spatial transformations using the em algorithm. In *IEEE Conference on Computer Vision and Pattern Recognition (CVPR)*, 1999. 2
- [26] Yaroslav Ganin, Daniil Kononenko, Diana Sungatullina, and Victor Lempitsky. Deepwarp: Photorealistic image resyn-

- thesis for gaze manipulation. In *European Conference on Computer Vision*, pages 311–326. Springer, 2016. 2
- [27] Ian Goodfellow, Jean Pouget-Abadie, Mehdi Mirza, Bing Xu, David Warde-Farley, Sherjil Ozair, Aaron Courville, and Yoshua Bengio. Generative Adversarial Nets. In *Advances in Neural Information Processing Systems (NeurIPS)*, 2014. 2
- [28] Erik Härkönen, Aaron Hertzmann, Jaakko Lehtinen, and Sylvain Paris. Ganspace: Discovering interpretable gan controls. *arXiv preprint arXiv:2004.02546*, 2020. 4
- [29] Kaiming He, Xiangyu Zhang, Shaoqing Ren, and Jian Sun. Deep residual learning for image recognition. In *IEEE Conference on Computer Vision and Pattern Recognition (CVPR)*, 2016. 13
- [30] Martin Heusel, Hubert Ramsauer, Thomas Unterthiner, Bernhard Nessler, and Sepp Hochreiter. Gans trained by a two time-scale update rule converge to a local nash equilibrium. In *Advances in Neural Information Processing Systems*, 2017. 16
- [31] G. B. Huang, V. Jain, and E. Learned-Miller. Unsupervised joint alignment of complex images. In *2007 IEEE 11th International Conference on Computer Vision*, 2007. 2
- [32] Minyoung Huh, Richard Zhang, Jun-Yan Zhu, Sylvain Paris, and Aaron Hertzmann. Transforming and projecting images to class-conditional generative networks. In *European Conference on Computer Vision (ECCV)*, 2020. 4
- [33] Eddy Ilg, Nikolaus Mayer, Tonmoy Saikia, Margret Keuper, Alexey Dosovitskiy, and Thomas Brox. FlowNet 2.0: Evolution of optical flow estimation with deep networks. In *Proceedings of the IEEE conference on computer vision and pattern recognition*, pages 2462–2470, 2017. 1
- [34] Max Jaderberg, Karen Simonyan, Andrew Zisserman, et al. Spatial transformer networks. In *Advances in Neural Information Processing Systems*, pages 2017–2025, 2015. 2, 3
- [35] Ali Jahanian, Xavier Puig, Yonglong Tian, and Phillip Isola. Generative models as a data source for multiview representation learning. *arXiv preprint arXiv:2106.05258*, 2021. 2
- [36] Xu Jia, Bert De Brabandere, Tinne Tuytelaars, and Luc V Gool. Dynamic filter networks. In *Advances in Neural Information Processing Systems*, pages 667–675, 2016. 2
- [37] Justin Johnson, Alexandre Alahi, and Li Fei-Fei. Perceptual losses for real-time style transfer and super-resolution. In *European Conference on Computer Vision (ECCV)*, 2016. 3
- [38] Angjoo Kanazawa, David W Jacobs, and Manmohan Chandraker. Warpnet: Weakly supervised matching for single-view reconstruction. In *Proceedings of the IEEE Conference on Computer Vision and Pattern Recognition*, pages 3253–3261, 2016. 2
- [39] Tero Karras, Timo Aila, Samuli Laine, and Jaakko Lehtinen. Progressive growing of gans for improved quality, stability, and variation. In *International Conference on Learning Representations (ICLR)*, 2018. 1, 8, 17
- [40] Tero Karras, Miika Aittala, Janne Hellsten, Samuli Laine, Jaakko Lehtinen, and Timo Aila. Training generative adversarial networks with limited data. *arXiv*, 2020. 7
- [41] Tero Karras, Samuli Laine, and Timo Aila. A style-based generator architecture for generative adversarial networks. In *IEEE Conference on Computer Vision and Pattern Recognition (CVPR)*, 2019. 1, 4, 8, 16, 17
- [42] Tero Karras, Samuli Laine, Miika Aittala, Janne Hellsten, Jaakko Lehtinen, and Timo Aila. Analyzing and improving the image quality of stylegan. In *Proceedings of the IEEE/CVF Conference on Computer Vision and Pattern Recognition*, pages 8110–8119, 2020. 4, 13
- [43] Ira Kemelmacher-Shlizerman and Steven M Seitz. Collection flow. In *Computer Vision and Pattern Recognition (CVPR), 2012 IEEE Conference on*, pages 1792–1799. IEEE, 2012. 2
- [44] Diederik Kingma and Jimmy Ba. Adam: A method for stochastic optimization. In *International Conference on Learning Representations (ICLR)*, 2015. 14
- [45] Nilesh Kulkarni, Abhinav Gupta, David F Fouhey, and Shubham Tulsiani. Articulation-aware canonical surface mapping. In *IEEE Conference on Computer Vision and Pattern Recognition (CVPR)*, 2020. 7, 8
- [46] Nilesh Kulkarni, Abhinav Gupta, and Shubham Tulsiani. Canonical surface mapping via geometric cycle consistency. *IEEE International Conference on Computer Vision (ICCV)*, 2019. 8
- [47] Erik G. Learned-Miller. Data driven image models through continuous joint alignment. *IEEE Trans. Pattern Anal. Mach. Intell.*, 28(2):236–250, 2006. 1, 2, 3
- [48] Chen-Hsuan Lin and Simon Lucey. Inverse compositional spatial transformer networks. In *IEEE Conference on Computer Vision and Pattern Recognition (CVPR)*, 2017. 2
- [49] Chen-Hsuan Lin, Ersin Yumer, Oliver Wang, Eli Shechtman, and Simon Lucey. St-gan: Spatial transformer generative adversarial networks for image compositing. In *Proceedings of the IEEE Conference on Computer Vision and Pattern Recognition*, pages 9455–9464, 2018. 2, 4
- [50] Yanbin Liu, Linchao Zhu, Makoto Yamada, and Yi Yang. Semantic correspondence as an optimal transport problem. In *Proceedings of the IEEE/CVF Conference on Computer Vision and Pattern Recognition (CVPR)*, June 2020. 1, 7
- [51] Ziwei Liu, Ping Luo, Xiaogang Wang, and Xiaoou Tang. Deep learning face attributes in the wild. In *IEEE International Conference on Computer Vision (ICCV)*, December 2015. 2, 5
- [52] Ilya Loshchilov and Frank Hutter. Sgdr: Stochastic gradient descent with warm restarts. *arXiv preprint arXiv:1608.03983*, 2016. 14
- [53] Bruce D. Lucas and Takeo Kanade. An iterative image registration technique with an application to stereo vision. In *Proceedings of the 7th International Joint Conference on Artificial Intelligence - Volume 2, IJCAI'81*, pages 674–679, 1981. 2
- [54] Chengzhi Mao, Augustine Cha, Amogh Gupta, Hao Wang, Junfeng Yang, and Carl Vondrick. Generative interventions for causal learning. In *Proceedings of the IEEE/CVF Conference on Computer Vision and Pattern Recognition*, pages 3947–3956, 2021. 2
- [55] Luke Melas-Kyriazi, Christian Rupprecht, Iro Laina, and Andrea Vedaldi. Finding an unsupervised image segmenter in each of your deep generative models. *arXiv preprint arXiv:2105.08127*, 2021. 2
- [56] Juhong Min and Minsu Cho. Convolutional hough matching networks. In *Proceedings of the IEEE/CVF Conference on*

- Computer Vision and Pattern Recognition (CVPR)*, pages 2940–2950, June 2021. 1, 7
- [57] Juhong Min, Jongmin Lee, Jean Ponce, and Minsu Cho. Hyperpixel flow: Semantic correspondence with multi-layer neural features. In *Proceedings of the IEEE/CVF International Conference on Computer Vision*, pages 3395–3404, 2019. 1, 7
- [58] Juhong Min, Jongmin Lee, Jean Ponce, and Minsu Cho. Spair-71k: A large-scale benchmark for semantic correspondence. *arXiv preprint arXiv:1908.10543*, 2019. 2, 7
- [59] Juhong Min, Jongmin Lee, Jean Ponce, and Minsu Cho. Learning to compose hypercolumns for visual correspondence. In *Computer Vision–ECCV 2020: 16th European Conference, Glasgow, UK, August 23–28, 2020, Proceedings, Part XV 16*, pages 346–363. Springer, 2020. 1, 7
- [60] Sangwoo Mo, Minsu Cho, and Jinwoo Shin. Freeze the discriminator: a simple baseline for fine-tuning gans. *arXiv preprint arXiv:2002.10964*, 2020. 7
- [61] Hossein Mobahi, Ce Liu, and William T. Freeman. A compositional model for low-dimensional image set representation. In *2014 IEEE Conference on Computer Vision and Pattern Recognition, CVPR 2014, Columbus, OH, USA, June 23–28, 2014*, pages 1322–1329. IEEE Computer Society, 2014. 2
- [62] Tom Monnier, Thibault Groueix, and Mathieu Aubry. Deep transformation-invariant clustering. In H. Larochelle, M. Ranzato, R. Hadsell, M. F. Balcan, and H. Lin, editors, *Advances in Neural Information Processing Systems*, volume 33, pages 7945–7955. Curran Associates, Inc., 2020. 2, 4
- [63] Eunbyung Park, Jimei Yang, Ersin Yumer, Duygu Ceylan, and Alexander C Berg. Transformation-grounded image generation network for novel 3d view synthesis. In *IEEE Conference on Computer Vision and Pattern Recognition (CVPR)*, 2017. 2
- [64] YiGang Peng, Arvind Ganesh, John Wright, Wenli Xu, and Yi Ma. RASL: robust alignment by sparse and low-rank decomposition for linearly correlated images. *IEEE Trans. Pattern Anal. Mach. Intell.*, 34(11):2233–2246, 2012. 2
- [65] Alec Radford, Luke Metz, and Soumith Chintala. Unsupervised representation learning with deep convolutional generative adversarial networks. In *International Conference on Learning Representations (ICLR)*, 2016. 2
- [66] Ignacio Rocco, Relja Arandjelovic, and Josef Sivic. Convolutional neural network architecture for geometric matching. In *Proceedings of the IEEE conference on computer vision and pattern recognition*, pages 6148–6157, 2017. 1, 7
- [67] Ignacio Rocco, Relja Arandjelović, and Josef Sivic. End-to-end weakly-supervised semantic alignment. In *Proceedings of the IEEE Conference on Computer Vision and Pattern Recognition*, pages 6917–6925, 2018. 1, 7
- [68] Ignacio Rocco, Mircea Cimpoi, Relja Arandjelović, Akihiko Torii, Tomas Pajdla, and Josef Sivic. Neighbourhood consensus networks. In *Advances in Neural Information Processing Systems*, volume 31, 2018. 1, 7
- [69] Paul Hongsuck Seo, Jongmin Lee, Deunsol Jung, Bohyung Han, and Minsu Cho. Attentive semantic alignment with offset-aware correlation kernels. In *Proceedings of the European Conference on Computer Vision (ECCV)*, pages 349–364, 2018. 1, 7
- [70] Karen Simonyan, Andrea Vedaldi, and Andrew Zisserman. Deep inside convolutional networks: Visualising image classification models and saliency maps. In *ICLR Workshop*, 2014. 8
- [71] Fabio Henrique Kiyoyiti dos Santos Tanaka and Claus Aranha. Data augmentation using gans. *arXiv preprint arXiv:1904.09135*, 2019. 2
- [72] Zachary Teed and Jia Deng. Raft: Recurrent all-pairs field transforms for optical flow. In *European Conference on Computer Vision*, pages 402–419. Springer, 2020. 1, 13
- [73] James Thewlis, Andrea Vedaldi, and Hakan Bilen. Unsupervised object learning from dense equivariant image labelling. In *Advances in Neural Information Processing Systems*, 2017. 8
- [74] Yu Tian, Jian Ren, Menglei Chai, Kyle Olszewski, Xi Peng, Dimitris N. Metaxas, and Sergey Tulyakov. A good image generator is what you need for high-resolution video synthesis. In *International Conference on Learning Representations*, 2021. 4
- [75] Antonio Torralba. <http://people.csail.mit.edu/torralba/gallery/>, 2001. 2
- [76] Nontawat Tritrong, Pitchaporn Rewatbowornwong, and Supasorn Suwajanakorn. Repurposing gans for one-shot semantic part segmentation. In *Proceedings of the IEEE/CVF Conference on Computer Vision and Pattern Recognition*, pages 4475–4485, 2021. 2
- [77] Shubham Tulsiani, Nilesh Kulkarni, and Abhinav Gupta. Implicit mesh reconstruction from unannotated image collections. 2020. 8
- [78] Grant Van Horn, Steve Branson, Ryan Farrell, Scott Haber, Jessie Barry, Panos Ipeirotis, Pietro Perona, and Serge Belongie. Building a bird recognition app and large scale dataset with citizen scientists: The fine print in fine-grained dataset collection. In *Proceedings of the IEEE Conference on Computer Vision and Pattern Recognition*, pages 595–604, 2015. 7
- [79] Andrey Voynov, Stanislav Morozov, and Artem Babenko. Big gans are watching you: Towards unsupervised object segmentation with off-the-shelf generative models. *arXiv preprint arXiv:2006.04988*, 2020. 2
- [80] C. Wah, S. Branson, P. Welinder, P. Perona, and S. Belongie. The Caltech-UCSD Birds-200-2011 Dataset. Technical Report CNS-TR-2011-001, California Institute of Technology, 2011. 2, 5
- [81] Eric Wu, Kevin Wu, David Cox, and William Lotter. Conditional infilling gans for data augmentation in mammogram classification. In *Image analysis for moving organ, breast, and thoracic images*, pages 98–106. Springer, 2018. 2
- [82] Xianglei Xing, Ruiqi Gao, Tian Han, Song-Chun Zhu, and Ying Nian Wu. Deformable generator network: Unsupervised disentanglement of appearance and geometry. *arXiv preprint arXiv:1806.06298*, 2018. 2
- [83] Xinchen Yan, Jimei Yang, Ersin Yumer, Yijie Guo, and Honglak Lee. Perspective transformer nets: Learning single-view 3d object reconstruction without 3d supervision. In *Advances in Neural Information Processing Systems*, pages 1696–1704, 2016. 2

- [84] Fisher Yu, Ari Seff, Yinda Zhang, Shuran Song, Thomas Funkhouser, and Jianxiong Xiao. Lsun: Construction of a large-scale image dataset using deep learning with humans in the loop. *arXiv preprint arXiv:1506.03365*, 2015. 2, 5
- [85] Richard Zhang, Phillip Isola, Alexei A Efros, Eli Shechtman, and Oliver Wang. The unreasonable effectiveness of deep features as a perceptual metric. In *IEEE Conference on Computer Vision and Pattern Recognition (CVPR)*, 2018. 8
- [86] Yuxuan Zhang, Wenzheng Chen, Huan Ling, Jun Gao, Yanan Zhang, Antonio Torralba, and Sanja Fidler. Image gans meet differentiable rendering for inverse graphics and interpretable 3d neural rendering. *arXiv preprint arXiv:2010.09125*, 2020. 2
- [87] Yuxuan Zhang, Huan Ling, Jun Gao, Kangxue Yin, Jean-Francois Lafleche, Adela Barriuso, Antonio Torralba, and Sanja Fidler. Datasetgan: Efficient labeled data factory with minimal human effort. In *Proceedings of the IEEE/CVF Conference on Computer Vision and Pattern Recognition*, pages 10145–10155, 2021. 2
- [88] Tinghui Zhou, Matthew Brown, Noah Snavely, and David G Lowe. Unsupervised learning of depth and ego-motion from video. *arXiv preprint arXiv:1704.07813*, 2017. 2
- [89] Tinghui Zhou, Yong Jae Lee, Stella Yu, and Alexei A Efros. Flowweb: Joint image set alignment by weaving consistent, pixel-wise correspondences. In *IEEE Conference on Computer Vision and Pattern Recognition (CVPR)*, 2015. 2
- [90] Tinghui Zhou, Shubham Tulsiani, Weilun Sun, Jitendra Malik, and Alexei A Efros. View synthesis by appearance flow. *ECCV*, 2016. 2
- [91] Jun-Yan Zhu, Philipp Krähenbühl, Eli Shechtman, and Alexei A. Efros. Generative visual manipulation on the natural image manifold. In *ECCV*, 2016. 4
- [92] Jun-Yan Zhu, Yong Jae Lee, and Alexei A Efros. Averageexplorer: Interactive exploration and alignment of visual data collections. *ACM Transactions on Graphics (TOG)*, 33(4):1–11, 2014. 2

A. Video Results

Please see our project page at www.wpeebles.com/gangealing for animated results, augmented reality applications and visual comparisons against other methods.

B. Implementation Details

Below we provide details regarding the implementation of GANgealing. Our code is also available at www.github.com/wpeebles/gangealing.

B.1. Spatial Transformer

Our full Spatial Transformer T is composed of two individual Spatial Transformers: T_{sim} —a network that takes an image as input and regresses and applies a similarity transformation to the input—and T_{flow} —a network that takes an image as input and regresses and applies an unconstrained dense flow field to the input. The warped output image produced by T_{sim} is fed directly into T_{flow} . Our final composed Spatial Transformer is given by $T = T_{\text{flow}} \circ T_{\text{sim}}$, where we compose the warps predicted by the two individual networks and apply it to the original input to obtain the final output.

The architectures of T_{sim} and T_{flow} are identical up to their final layers. Specifically, they each use a ResNet backbone [29], closely following the design of the ResNet-based discriminator from StyleGAN2 [42]; in particular, we do not use normalization layers. We do *not* use weight sharing for any layers of the two networks, and both modules are trained together jointly from scratch.

Similarity Spatial Transformer. The final parametric layer of T_{sim} takes the spatial features produced by the ResNet backbone, flattens them, and sends them through a fully-connected layer with four output neurons o_1, o_2, o_3 and o_4 . We construct the affine matrix M representing the similarity transform as follows:

$$r = \pi \cdot \tanh(o_1) \tag{7}$$

$$s = \exp(o_2) \tag{8}$$

$$t_x = o_3 \tag{9}$$

$$t_y = o_4 \tag{10}$$

$$M = \begin{bmatrix} s \cdot \cos(r) & -s \cdot \sin(r) & t_x \\ s \cdot \sin(r) & s \cdot \cos(r) & t_y \\ 0 & 0 & 1 \end{bmatrix} \tag{11}$$

To obtain the warped output image, we apply the affine matrix M to an identity sampling grid, and apply the resulting transformed sampling grid to the input.

Unconstrained Spatial Transformer. The features produced from T_{flow} 's ResNet backbone have spatial resolution 16×16 . These features are fed into two separate, small

convolutional networks: (1) a network that outputs a coarse flow of spatial resolution 16×16 with 2 channels (the first channel contains the horizontal flow while the second contains the vertical flow); (2) a network that outputs weights used to perform learned convex upsampling as described in RAFT [72]. Both of these networks consist of two conv layers (each with 3×3 kernels and unit padding) with a ReLU in-between. After performing $8 \times$ convex upsampling on the coarse flow, we obtain our higher resolution flow $\mathbf{g}_{\text{dense}}$ of resolution 128×128 . This flow field can be further densified with any type of interpolation.

In the case of the composed Spatial Transformer, we directly compose $\mathbf{g}_{\text{dense}}$ with the affine matrix M predicted by T_{sim} . We then sample from the original, unwarped input image according to this composed flow.

B.2. Clustering

For the clustering-variant of GANgealing ($K > 1$), our architectures as described above are only slightly changed as follows. T_{sim} 's final fully-connected layer has $4K$ output neurons that are used to build a total of K affine matrices $\{M_k\}_{k=1}^K$, one warp per cluster.

Similarly, the only change to T_{flow} is that the two convolutional networks at the end of the network each have K times as many output channels—each cluster predicts its own coarse-resolution 16×16 flow and its own set of weights used for convex upsampling.

Cluster Initialization. In contrast to the $K = 1$ case (where we initialize \mathbf{c} as $\bar{\mathbf{w}}$, the average \mathbf{w} vector), we randomly-initialize the \mathbf{c}_i . We do this using K -means++ [5] (only the initialization part). In standard K -means++, one selects centroids from points in the input dataset. In our case, we generate a pool of 50,000 random \mathbf{w} vectors to apply K -means++ to. The first centroid \mathbf{c}_0 is selected uniformly at random from the pool. Recall that K -means++ requires a distance function so it can gauge how well-represented the points in the pool are by the currently selected centroids. We define the distance between two latent vectors as $d(\mathbf{w}_1, \mathbf{w}_2) = \ell(G(\text{mix}(\mathbf{w}_1, \bar{\mathbf{w}})), G(\text{mix}(\mathbf{w}_2, \bar{\mathbf{w}})))$. The motivation for feeding-in $\bar{\mathbf{w}}$ into the later layers of StyleGAN is to ensure that the two latents are being compared based on the poses they represent when decoded to images, *not* the appearances they represent.

B.3. Smoothly-Congeaed Target Images

	PCK@ $\alpha_{\text{bbox}} = 0.1$
w/o target annealing	59.3%
w/ target annealing	67.2%

Table 4. The effects of smooth target annealing for LSUN Cats. Smooth target annealing improves GANgealing performance.

A significant benefit of GAN-Supervision is that it naturally admits a smooth learning curriculum. Rather than force T to learn the (often complex) mapping from \mathbf{x} to \mathbf{y} at the onset of training, we can instead smoothly vary the latent vector used to generate the target \mathbf{y} from \mathbf{w} to $\text{mix}(\mathbf{c}, \mathbf{w})$. Early in training, $\mathbf{y} \approx \mathbf{x}$ and T thus only has to learn very small warps where there are large regions of overlap between its input and target. As training proceeds, we gradually anneal the target latent $\mathbf{w} \rightarrow \text{mix}(\mathbf{c}, \mathbf{w})$ with cosine annealing [52] over the first 150,000 gradient steps. As this occurs, the learned \mathbf{y} target images gradually become aligned across all \mathbf{w} and require T to predict increasingly intricate warps. As shown in Table 4, excluding this smooth annealing degrades performance from 67.2% to 59.3%.

B.4. Horizontal Flipping

Because T_{sim} regresses the log-scale of a similarity transformation (o_2), it is incapable of performing horizontal flipping. While T_{flow} is in principle capable of learning how to horizontally (or vertically) flip an image, in practice, we find that it is beneficial to explicitly parameterize horizontal flips. We found two methods effective.

Unimodal Models. Our unimodal models ($K = 1$) are not trained with any flipping mechanism, and we introduce the capability only at test time. This is done with the flow smoothness trick as described above in Appendix G.2—we query T with both \mathbf{x} and $\text{flip}(\mathbf{x})$, choosing whichever yields the smoothest flow field. This simple heuristic is surprisingly reliable.

Clustering Models. Clustering models provide a slightly more direct way to handle flipping. During training, when we evaluate the perceptual reconstruction loss on an input fake image $G(\mathbf{w})$, we also evaluate the loss on $\text{flip}(G(\mathbf{w}))$ (the loss is computed against $\mathbf{y} = G(\text{mix}(\mathbf{c}, \mathbf{w}))$ for both inputs). We only optimize the minimum of those two losses. At test time, we need to train a classifier to predict whether an input image should be flipped. To this end, we have the cluster classifier (as described in Section 3.2) directly predict both cluster assignment as well as whether or not the input should be flipped by simply doubling the number of output classes.

B.5. Training Details

As with most Spatial Transformers, we initialize the final output layers of our networks such that they predict the identity transformation. For T_{sim} , this is done by initializing the final fully-connected matrix as the zeros matrix (and zero bias); for T_{flow} , the convolutional kernel that outputs the coarse flow is set to all-zeros.

We jointly optimize the loss with respect to both T and \mathbf{c} using Adam [44] (we do not use alternating optimization).

Dataset	\mathcal{W}^+ cutoff	N	K	GAN Resolution
LSUN (unimodal)	5	1	1	256×256
CUB	5	1	1	256×256
LSUN (clustering)	6	5	4	256×256
In-The-Wild CelebA	6	512	1	128×128

Table 5. GANgealing Hyperparameters.

We use a learning rate of 0.001 for T and a learning rate of 0.01 for \mathbf{c} . We apply the cosine annealing with warm restarts scheduler [52] to both learning rates. We use a batch size of 40. Finally, we note that we do not make use of any data augmentation—GANgealing uses raw samples directly from the generator as the training data.

B.6. Hyperparameters

We use $\lambda_{TV} = 2500$ for all models trained with LPIPS and $\lambda_{TV} = 1000$ for all models trained with the self-supervised perceptual loss. All models use $\lambda_I = 1$. We detail other hyperparameters in Table 5.

N controls how many degrees of freedom \mathbf{c} has in choosing the target pose that T congeals towards. As shown in Table 3, small N are *critical* for some models (LSUN Cats with $N = 512$ gets less than 1% PCK on SPair Cats whereas $N = 1$ achieves 67%). However, StyleGAN2 generators with less expressive \mathcal{W} spaces (such as those trained on In-The-Wild CelebA) can function well without any constraints ($N = 512$).

Padding Mode. One subtle hyperparameter is the padding mode of the Spatial Transformer which controls how T samples pixels beyond image boundaries. We found that `reflection` padding is the “safest” option and seems to work well in general. We also found `border` padding works well on some datasets (e.g., LSUN Cats and Dogs, CUB, In-The-Wild CelebA), but can be more prone to degenerate solutions on datasets like LSUN Bicycles and TVs. We recommend `reflection` as a default choice.

B.7. Direct Image-to-Image Correspondence

Our method is able to find dense correspondences directly between any pair of images \mathbf{x}_A and \mathbf{x}_B . Figure 8 gives an overview of the process. At a high-level, this merely involves applying the forward warp that maps points in \mathbf{x}_A to points in $T(\mathbf{x}_A)$ and composing it with the reverse warp that maps points in the congealed coordinate space back to \mathbf{x}_B . We go into detail about this procedure in this section.

Recall that T outputs a sampling grid \mathbf{g} which maps points in congealed space to points in the input image. Without loss of generality, say we wish to know where a point (i, j) in \mathbf{x}_A corresponds to in \mathbf{x}_B . First, we need to determine where (i, j) maps to in the congealed image $T(\mathbf{x}_A)$ —i.e., we need to *congeal* point (i, j) . This is given by the value at pixel coordinate (i, j) in the **inverse** of the sampling

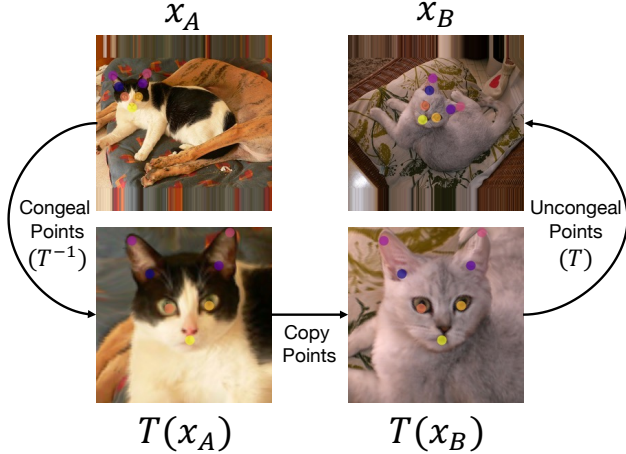


Figure 8. The process for finding correspondences between two images with GANgealing.

grid produced by T for x_A . When T produces similarity transformations, we can analytically compute this inverse by inverting the affine matrix representing the similarity transform and applying it to the identity sampling grid. Unfortunately, for the unconstrained flow case we cannot analytically determine \mathbf{g}^{-1} . There are many ways one could go about obtaining this inverse. We opt for the simplest solution—inversion via nearest neighbors. Specifically, we can approximate the quantity by using nearest neighbors to find the pixel coordinates that give rise to the coordinates closest to (i, j) in \mathbf{g} . Recall that $\mathbf{g}_{i,j}$ is the input pixel coordinate that gets mapped to pixel (i, j) in congealed coordinate space. Then we can approximate $\mathbf{g}_{i,j}^{-1} \approx \arg \min_{i',j'} \|\mathbf{g}_{i',j'} - [i, j]\|_2$.

Now that we know where points in x_A map to in $T(x_A)$, the last step is to determine where the congealed points ($\mathbf{g}_{i,j}^{-1}$) map to in x_B —i.e., we need to *uncongeal* $\mathbf{g}_{i,j}^{-1}$. This is the easy step: we need only query the sampling grid (produced by applying T to x_B) at location $\mathbf{g}_{i,j}^{-1}$.

C. Clustering Results

Figure 9 shows our $K = 4$ learned clusters for our LSUN Cars and Horses models. We show dense correspondence results for various clusters in Figure 10.

D. Visualizing GAN-Supervised Training Data

We show examples of our paired GAN-Supervised training data in Figure 11. In Table 3, we showed that learning the fixed mode can be essential for some datasets (e.g., LSUN Cats). Figure 11 illustrates one potential reason why it is so critical: often, the initial truncated target mode in StyleGAN2 models produces *unrealistic* images. For example, truncated bicycles are surrounded with incoherent texture and have an unnatural structure, truncated TVs are unintelli-

gible and truncated cats have unnatural bodies. Congealing all images to these poor targets could produce erroneous correspondences; hence, *learning* the target mode is in general very important.

Furthermore, the initial mode is often unsuitable as a dataset-wide congealing target. For example, not all LSUN Cat images (real or fake) feature the full-body of a cat, but most do feature a cat’s upper-body. Hence, GANgealing updates the target to a more suitable target “reachable” by the broader distribution. Finally, also observe that our Spatial Transformer can be successfully trained even in the presence of *imperfect targets*: the target bicycles sometimes do not retain the color of the corresponding input fake bicycle, for instance.

E. Accelerating GAN Training with Learned Pre-Processing

A natural application of GANgealing is unsupervised dataset alignment for downstream machine learning tasks. In this section, we use our trained Spatial Transformer networks to align and filter data for GAN training.

Filtering. The first step is dataset filtering. We would like to remove two types of images: (1) images for which our Spatial Transformer makes a mistake (i.e., produces an erroneous alignment) and (2) images that are *unalignable*. For example, several images in LSUN Cats do not actually contain any cats. And, some images contain cats that cannot be well-aligned to the target mode (e.g., due to significant out-of-plane rotation of the cat’s face). We can automatically detect these problematic images by examining the *smoothness* of the flow field produced by the Spatial Transformer for a given input image: images with highly un-smooth flows usually correspond to one of these types of problematic images. Please refer to Appendix G.2 below for a detailed explanation of this procedure. Here, we experiment with dropping 75% of real images (those with the least-smooth flow fields), reducing LSUN Cats’ size from 1,657,264 images to 414,316 images.

Alignment. The second step is to align the filtered dataset. This is done by applying our Spatial Transformer to congeal every image in the input dataset. To avoid introducing excessive warping artifacts into the output distribution, we only use our similarity Spatial Transformer T_{sim} (which performs oriented cropping) in this step—we merely remove the unconstrained T_{flow} Spatial Transformer module from our trained T . To ensure a high quality output dataset, we remove some additional images during this procedure. (1) We removes images for which T_{sim} has to extrapolate a large number of pixels beyond image boundaries to avoid output images with lots of visible padding. (2) We remove images

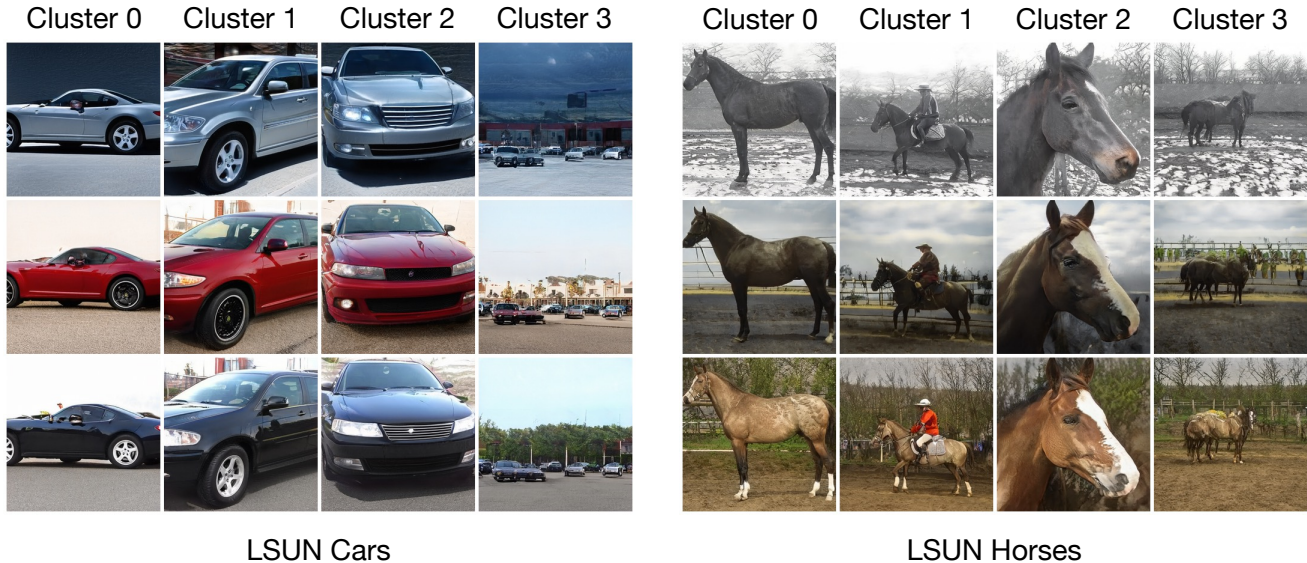


Figure 9. **Learned clusters.** We show three samples of target images y at the end of training which define our $K = 4$ learned clusters.

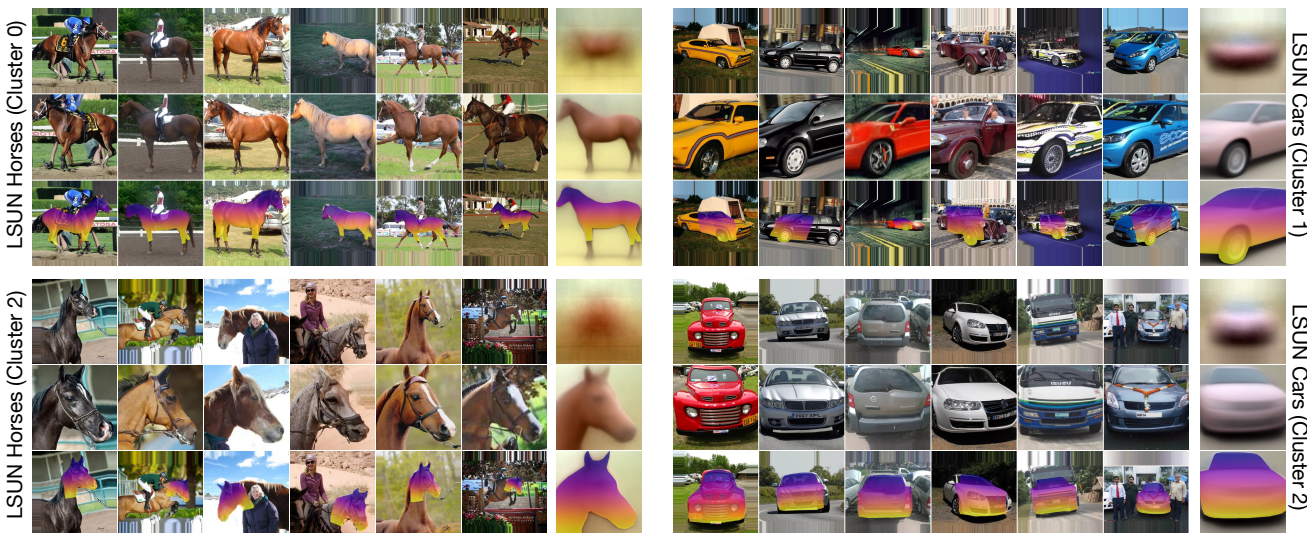


Figure 10. **Dense correspondence results for different clusters.** For each cluster, the top row shows unaligned real images assigned to that cluster by our cluster classifier; we also show the cluster’s average image. The middle row shows our learned transformations of the input images. The bottom row shows dense correspondences between the images.

where T_{sim} zooms-in “too much.” The motivation for this second criterion is that some images contain very small objects, and in these cases the congealed image will be low resolution (blurry). These two heuristics further reduce dataset size from 414,316 images to 58,814 high quality aligned images.

Quantitative Results. We apply our learned pre-processing procedure to the LSUN Cats dataset for downstream GAN training. As is common practice when training GANs on aligned datasets like AFHQ and FFHQ,

we use mirror augmentations [41] when training on our aligned data. In Figure 12, we show that training with our learned pre-processing enables GANs to converge to good FID [30] faster by simplifying the training distribution. We also show that while *only* filtering the dataset to 58,814 images without alignment accelerates convergence (a conclusion similar to the one found by DeVries et. al [18]), both steps together provide the greatest speed-up. We stress that our gains in Figure 12 come from *simplifying the training distribution*. We leave showing how learned

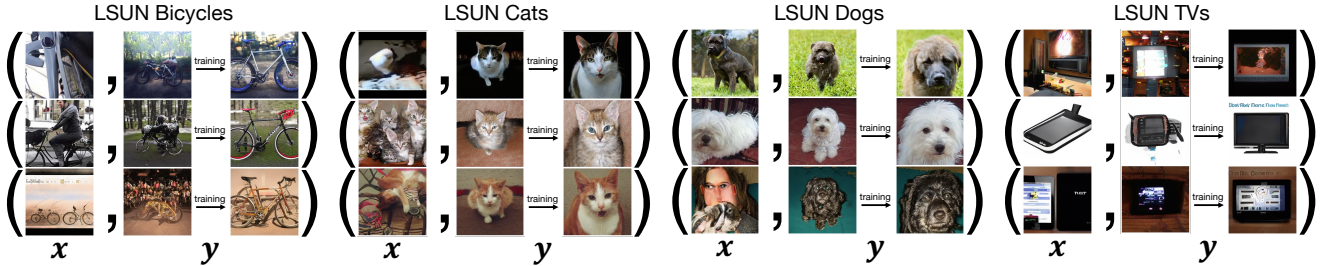


Figure 11. **Examples of GAN-Supervised paired data used in GANgealing.** For each dataset, we show random GAN samples $x = G(\mathbf{w})$ used to train our Spatial Transformer. For each input x , we show both the *initial* target image $y = G(\text{mix}(\mathbf{c} = \bar{\mathbf{w}}, \mathbf{w}))$ as well as our *learned* target at the end of training $y = G(\text{mix}(\mathbf{c}, \mathbf{w}))$. The initial target images (initialized with the truncation trick) are often unrealistic—for example, the initial LSUN TV targets are largely incoherent. Learning \mathbf{c} is essential so images can be congealed to a coherent target. Note that we omit target annealing (Appendix B.3) in this visualization for clarity.

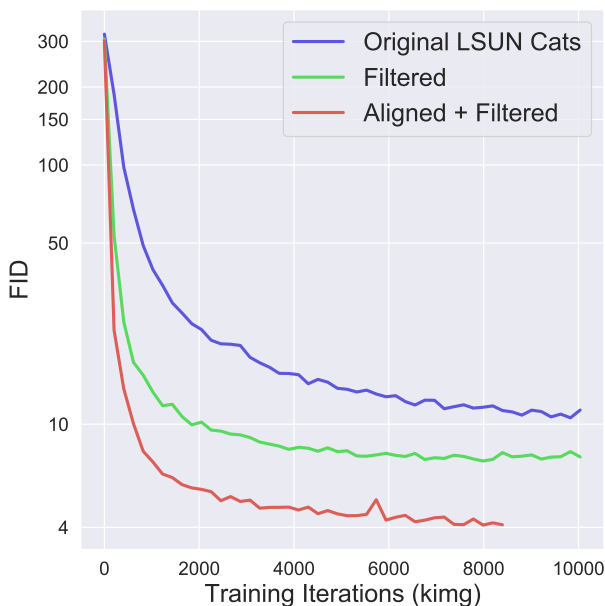


Figure 12. **The effect of aligning and filtering datasets before GAN training.** Each curve represents a StyleGAN2 trained on LSUN Cats with different data pre-processing. For each model, we compute FID against its corresponding pre-processed real distribution (i.e., the Original LSUN Cats curve computes FID against LSUN Cats, Filtered LSUN Cats computes FID against the filtered LSUN Cats distribution, etc.). Aligning and filtering images with our method yields significantly better FID early in training by simplifying the real distribution.

alignment can improve performance on the original, unaligned distribution to future work. Given the extent to which human-supervised dataset alignment and filtering is prevalent in the GAN literature [15, 39, 41], we hope our unsupervised procedure will be used in the future to automate these important steps.

Visual Results. In Figure 13 we show 96 uncurated, untruncated GAN samples for the baseline LSUN Cats model (FID versus LSUN Cats is 6.9); in Figure 14 we show uncurated samples from a StyleGAN2 trained on our learned aligned and filtered LSUN Cats (FID versus pre-processed LSUN Cats is 3.9). Our learned alignment improves the visual fidelity of the generator by reducing the complexity of the real distribution through alignment and filtering.

F. Uncurated Dense Correspondence Results

Below we show 120 *uncurated* dense correspondence results for each of our eight datasets. The results are best viewed zoomed-in.

G. Emergent Properties of GANgealing

We empirically find that our Spatial Transformer develops two useful test time capabilities from training with GANgealing.

G.1. Recursive Alignment

Recall that our Spatial Transformer consists of two sub-modules: a similarity warping Spatial Transformer T_{sim} and an unconstrained Spatial Transformer T_{flow} . Once trained, we find that T_{sim} 's primary role is to localize objects and correct in-plane rotation; T_{flow} brings the localized object into tight alignment by handling articulations, out-of-plane rotation, etc. For especially complex datasets (e.g., all LSUN categories), objects appear at many scales and are sometimes non-trivial to accurately localize. Surprisingly, we find that the T_{sim} network can be applied *recursively* multiple times to its own output at test time, significantly improving the ability of T to accurately align challenging images. This recursive processing appears to be relatively stable—i.e., T does not explode as we increase the number of recursions. We use three recursive iterations of T_{sim} for our LSUN models.

We suspect the reason this behavior emerges is because, over the course of training, it is likely that many generated in-

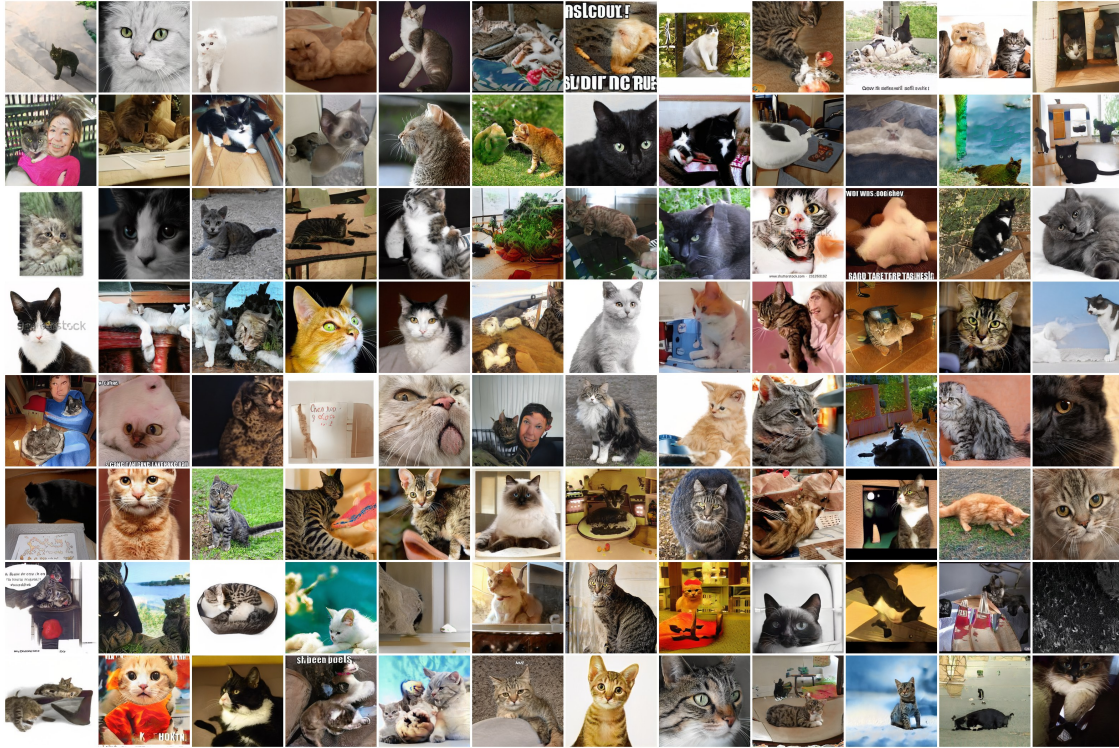


Figure 13. Uncurated samples from an LSUN Cats StyleGAN2.

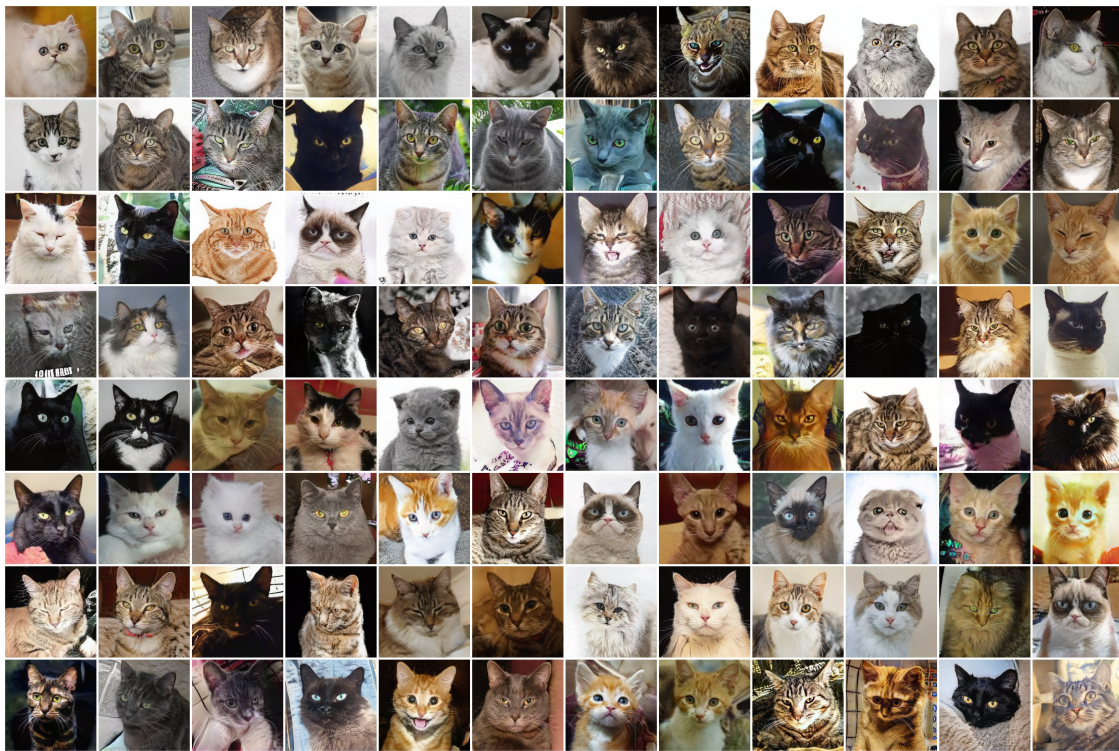


Figure 14. Uncurated samples from a StyleGAN2 trained on LSUN Cats pre-processed with our learned alignment and filtering. Our method leads to a GAN with higher overall visual fidelity at the cost of reduced dataset complexity.



Figure 15. LSUN Bicycles uncurated results.

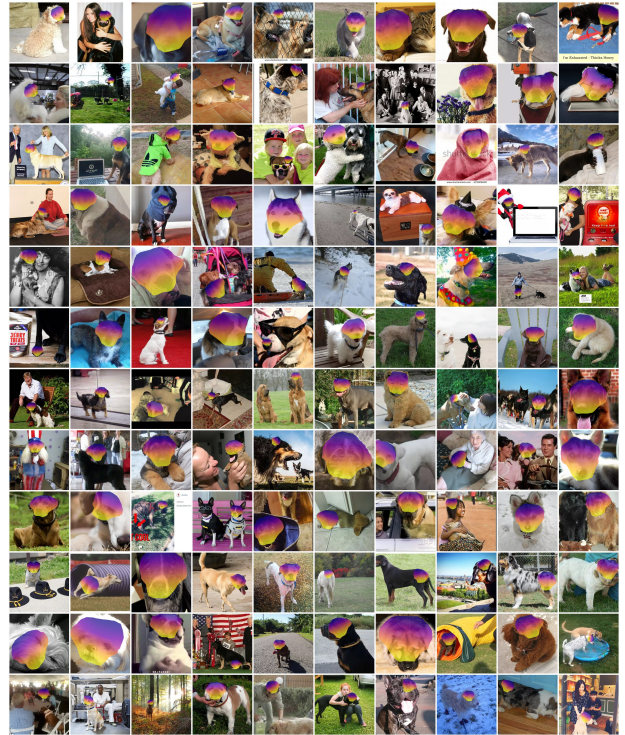


Figure 17. LSUN Dogs uncurated results.

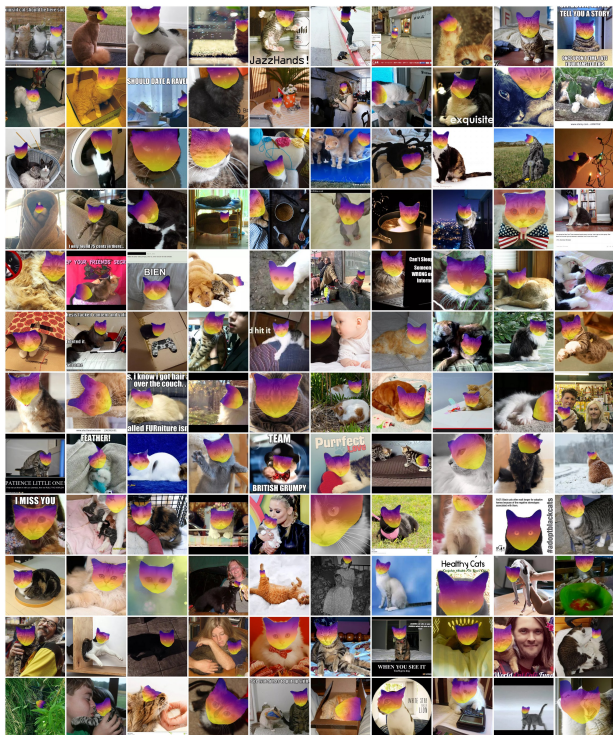


Figure 16. LSUN Cats uncurated results.

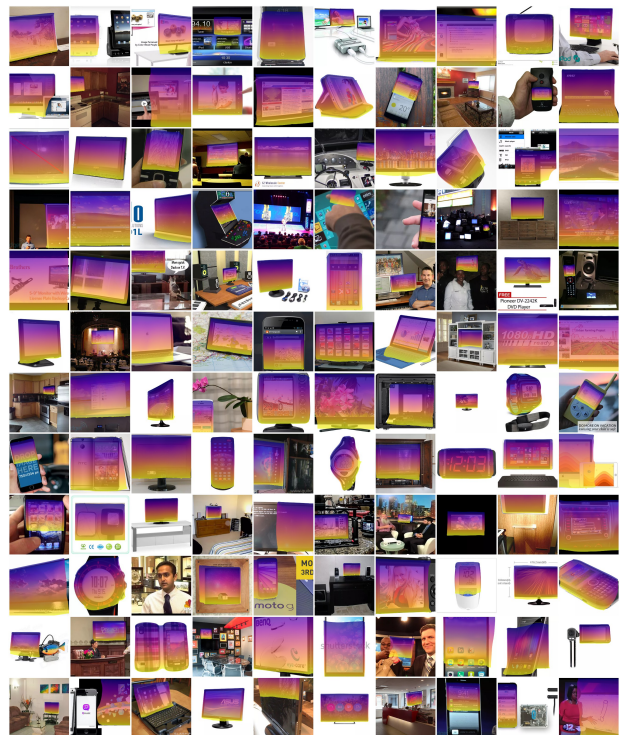


Figure 18. LSUN TVs uncurated results.

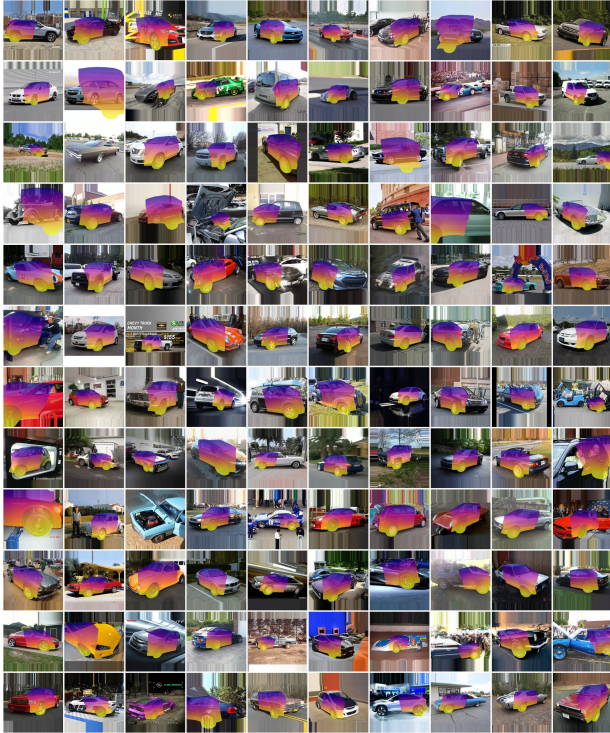


Figure 19. LSUN Cars (cluster 1) uncurated results.



Figure 21. In-The-Wild CelebA results. The results are uncurated with the exception of replacing three potentially offensive images.



Figure 20. LSUN Horses (cluster 0) uncurated results.

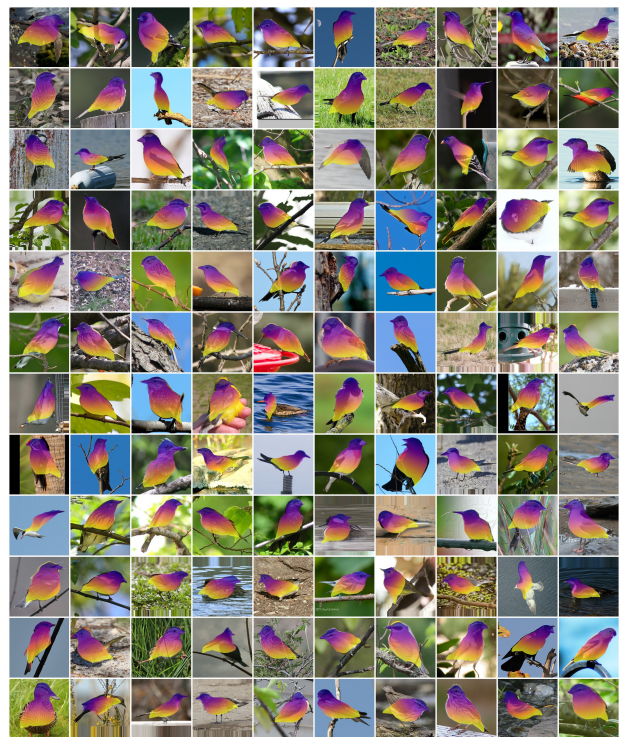


Figure 22. CUB uncurated results.



Figure 23. **GANgealing produces high frequency flow fields for unalignable images.** Each image in the top row shows a cat that either cannot be congealed to the learned mode or is a failure case of the Spatial Transfer. Our T produces high frequency flows to try and “fool” the perceptual loss for these hard cases. These examples are easily detected.

puts x will be sampled that are close to the target y . In other words, it is likely that w get sampled such that $w \approx c^3$, and hence the Spatial Transformer must learn to produce approximately the identity function in these cases. Thus, aligned fake images happen to be *in-distribution* for T , meaning it can stably process increasingly aligned real images at test time without issue in this recursive evaluation.

G.2. Flow Smoothness

A particularly useful behavior developed by our T is a tendency to *fail loudly*. What happens when T is faced with an unalignable image or makes a mistake? As shown in Figure 23, T produces very high-frequency flow fields to try and fool the perceptual loss (e.g., by synthesizing cat ears and eyes from background texture). It turns out these failure cases are easily detectable by simply measuring how smooth the flow field produced by T is—this can be done by evaluating our \mathcal{L}_{TV} total variation loss on the flow. This behavior enables several test time capabilities; for example, we can determine if an image should be horizontally flipped by merely running x and $\text{flip}(x)$ through T and selecting whichever input yields the smoothest flow. Or, we can score real images by their flows’ \mathcal{L}_{TV} and drop a percentage of the dataset with the worst (most positive) scores—this is how we perform dataset filtering with our T as part of our learned pre-processing for downstream GAN training as described above in Appendix E.

H. Broader Impacts

As with all machine learning models, our Spatial Transformer is only as good as the data on which it is trained. In the case of GANgealing, this means our algorithm’s success in finding correspondence depends on the underlying generative model which generates its training data. Concern

³This is likely *as long as c is properly constrained*. When poorly constrained, c may correspond to an *out-of-distribution* image and hence T may not be used to processing images similar to sampled y . Indeed, for our In-The-Wild CelebA model where $N = 512$ (i.e., c is not constrained at all), we find recursion is unstable. For all LSUN models where $N \leq 5$, we find it helps significantly.

over GANs’ tendency to drop modes is well-documented (e.g., [9]). However, as latent variable generative models continue to improve—including efforts to improve mode coverage—we expect that GANgealing will improve as well.

I. Assets

Here we list links to the assets used in Figures 1 and 4 (object propagation):

- [Cat Batman Mask](#)
- [Bird Soldier](#)
- [Rudolph Dog](#)
- [CelebA Pokémon Tattoo 1](#)
- [CelebA Pokémon Tattoo 2](#)
- [Unicorn Horn](#)
- [Horse Saddle](#)
- [Car Dragon Decal](#)